Musa acuminata peel extract assisted green Synthesis of ZnO/CuO Nanocomposite for Photocatalytic Degradation of Methylene Blue Dye

By: Mekedes Tenkolu

A Thesis Submitted to Department of Applied Chemistry

School of Applied Natural Science

In Partial Fulfillment of the Requirements for the Degree of

Master of Science in Chemistry (Physical Chemistry)

Office of Graduate Studies

Adama Science and Technology University

Adama, Ethiopia

October, 2020

Musa acuminata peel extract assisted green Synthesis of ZnO/CuO Nanocomposite for Photocatalytic Degradation of Methylene Blue Dye

By: Mekedes Tenkolu

Major advisor: Fedlu Kedir (PhD)

Co - advisor: Bedasa Abdisa (PhD)

A Thesis Submitted to the Department of Applied Chemistry

School of Applied Natural Science

In Partial Fulfillment of the Requirements for the Degree of

Master of Science in Chemistry (Physical Chemistry)

Office of Graduate Studies

Adama Science and Technology University

Adama, Ethiopia

October, 2020

Candidate Declaration

I declare that the work which is being presented in this research entitled as ‘‘*Musa acuminata* peel extract assisted green Synthesize of ZnO/CuO Nanocomposite for Photocatalytic Degradation of Methylene Blue Dye’’ and submitted in the partial fulfillment of the requirements for Master of Science in applied Chemistry (Physical Chemistry) complies with the regulation of the university and meets the accepted standards with respect to originality and quality of the thesis work. It was authentic record of my original work carried out from October 2019 to September, 2020 under the advisor of Dr. Fedilu Kedir and Dr. Bedasa Abdisa, Department of Applied Chemistry, School of Applied Natural Science, Adama Science and Technology University. The matter embodied in this has not been submitted by other person or me for the award of any other degree. All relevant resources of information used in this body have been duly acknowledged

Mekedes Tenkolu Maru

Signature: _____

This thesis has been submitted for examination with my approval as a University advisor and co-advisor.

Advisor: Dr. Fedilu Kedir

Signature: _____

Co-advisor: Dr. Bedasa Abdisa

Signature: _____

Approval sheet

ADAMA SCIENCE AND TECHNOLOGY UNIVERSITY

SCHOOL OF APPLIED NATURAL SCIENCE

DEPARTMENT OF APPLIED CHEMISTRY

M.Sc. PROGRAM

This is to certify that the thesis prepared by Mekedes Tenkolu, entitled ‘‘*Musa acuminata* peel extract assisted green Synthesize of ZnO/CuO Nanocomposite for Photocatalytic Degradation of Methylene Blue Dye’’ and submitted in the partial fulfillment of the requirements for Master of Science in applied Chemistry (Physical Chemistry) complies with the regulation of the university and meets the accepted standards with respect to originality and quality of the thesis work.

Name of a student	signature	date
---	---	---
Advisors name	signature	date
---	---	---
Co-advisor	signature	date
---	---	---

External examiner	signature	date
Dr. Endale Tsegaye		
Internal examiner	signature	date
---	---	---
Chairman	Signature	date
---	---	---
Department head	signature	date
---	---	---
School Dean	signature	date
---	---	---
Postgraduate Dean	signature	date
---	---	---

Acknowledgment

First and foremost, I would like to thank the only almighty God, the embodiment of wisdom who provides health, strength and accurate insight into reality for his divine intervention during my research work.

Although this thesis work ultimately represents my accomplishments, I have benefited significantly from multiple peoples that I would like to acknowledge. First and foremost, I am grateful to goes to my hard-working advisors: Dr. Fedlu Kedir and Dr. Bedasa Abdisa for their excellent supervision and scientific input in this research work. It is a great privilege and honor for me to be advised by them. I owe special thanks to my mentor, Dr. Fedlu Kedir, whose unique scientific passion and extensive knowledge I strongly admire and will always aspire to achieve; his patience, daily guidance and support have kept me on the right track all the way to the end. His positive influence will always be a guide as I venture out on my own to tackle challenging scientific problems. I am lucky to be guided and advised by him and in general his friendly approach makes me a successful man.

Then I would like to express my genuine heartfelt gratitude to my co-advisor, Dr. Bedasa Abdisa for his invaluable suggestion, comments, corrections, professional & technical guidance throughout my work for the successful accomplishment of this thesis.

I would like to express my sincere gratitude to all academic, technical and support staff of the Program of Applied Chemistry, Adama Science and Technology University, for providing the necessary knowledge, assistance and facilities to conduct my research work. Finally, I would like to thank greatly Adama Science and Technology University for giving me the opportunity to join this postgraduate program and for free sponsorship of my study.

Abstract

Photocatalytic degradation of organic pollutants is an environmentally friendly technique for water treatment. In this study, ZnO NPs, CuO NPs and ZnO/CuO photocatalyst with CuO weight percent (w/w%) of 10%,15%,20% and 25% were successfully synthesized *via* sol-gel method using *Musa acuminata* peel extract as capping and reducing agent. The synthesized NPs and nanocomposites were characterized by thermogravimetric analysis (TGA/DTA), X-ray diffraction (XRD), scanning electron microscopy (SEM), UV–vis diffuse reflectance spectroscopy (UV-DRS) and Fourier transform infrared (FTIR) spectroscopy. The XRD analysis showed the synthesized NPs and nanocomposites are well crystalline without any impurity. The SEM studies revealed cotton-like porous morphology for ZnO/CuO nanocomposites which is helpful for photocatalysis. The UV-DRS studies revealed that bandgap energy (Eg) of ZnO is narrowed from 3.24 eV to 3.05 eV as CuO is coupled with it. The photocatalytic activities of ZnO, CuO and ZnO/CuO nanocomposites were evaluated by the degradation of Methylene blue dye under visible light irradiation. The results indicated 57%, 50% and 90% degradation efficiency of MB for ZnO, CuO and ZnO/CuO respectively. Furthermore, parameters such as effect of pH of the dye solution, catalyst loading and dye concentration were also studied.

List of figures

List of tables

List of acronyms

AOPS	Advanced Oxidation Process
Eg	Bandgap Energy
BP	Banana peel
BG	Bromocresol green
BET	Brunauer–Emmett–Teller
CB	Conduction band
DTA	Differential thermal analysis
DRS	Diffuse reflectance spectra
eV	Electron volt
FTIR	Fourier Transform Infrared
IC	Indigo Carmine
JCPDS	Joint Committee on Powder Diffraction Standards
MB	Methylene Blue
MO	Methyl orange
MG	Methyl green
NPs	Nanoparticles
PL	Photoluminescence
Ppm	Parts per million
RB	Rose Bengal
Rho-B	Rhodamine B
SEM	Scanning electron microscopy
TGA	Thermo Gravimetric Analysis
TEM	Transmission electron microscopy
UV-VIS	Ultra Violet Visible
VB	Valence band
XRD	X-ray Powder Diffraction
ZC	Zinc copper

1. Background

1.1. Introduction

The intensification of human activities associated with economic development has caused the increase of waste generation and the pollution of water bodies. The textile industries, for instance, use highly reactive dyes, such as methylene blue and methyl orange, which are harmful to the environment due to their high carcinogenic and mutagenic potential [1]. When discarded without adequate treatment, they can change the color of water bodies, promoting significant changes in the hydrological cycle [2]. Thus, the degradation of organic dyes is of great environmental and industrial importance. Miscellaneous methods such as ion exchange [3], reverse osmosis [4], membrane filtration [5], adsorption processes [6], chlorination [7] and chemical precipitation have been widely explored for water treatment but cannot completely degrade the organic pollutants. Recent studies have shown that advanced oxidation process (AOPs) using heterogeneous photo-catalysis are the best alternative to conventional methods [8] due to its relative low-cost and high stability, nontoxicity, absence of resistance to mass transfer and secondary pollution, operation under ambient conditions, and more importantly the potential for decomposing the recalcitrant organic pollutants at short reaction time into less harmful compounds [9].

One of AOPs is heterogeneous photocatalysis using semiconducting metal oxides nanoparticles. In this process the electron hole pairs degrade the dye molecules in the water in to less harmful components [10]. Currently metal-oxide nanoparticles such as titanium (IV) oxide (TiO_2), zinc (II) oxide (ZnO), iron (III) oxide (Fe_2O_3), and tin (IV) oxide (SnO_2) have explored to be used as photocatalyst. Among these metal oxide nanoparticles, TiO_2 and ZnO are known as the most prominent semiconductor photo-catalyst since both have relatively high photocatalytic activities, exhibit excellent thermal, biological, and chemical stabilities and long lifespans, non-toxic and inexpensive [11]. Several reports confirmed that ZnO is preferred over TiO_2 for the photo-catalytic degradation of pollutant due to its high quantum efficiency [12]. However, ZnO is a wide direct band gap semiconductor. As a photo-catalytic material, it shows two obvious defects:(1) The recombination efficiency of photo-generated electrons and holes is high; (2) ZnO can absorb only

the ultraviolet light with energy higher than the band gap value. Theses draw backs must be overcome to enhance the photo-catalytic performance of ZnO NPs [13].

To enhancement photo-catalytic activity of ZnO NPs, modification techniques such as doping of metal and nonmetal and coupling with other semiconductor is done so far [13]. Among this, coupling with p-type CuO semiconductor is preferable to enhance the photo-catalytic activity of ZnO by inhibiting charge carrier recombination and extending the absorption to visible region due to the low band gap of the CuO which is in the visible range (1.2-2.4eV) [14].

Several methods have been used for metal oxide nanocomposite synthesis such as hydrothermal [15], electrochemistry [16], wet chemical [17], microwave method [17], co precipitation, sol–gel, wet impregnation, and thermal decomposition [18]. However, these classical methods to synthesize metal oxide nanoparticles using hazardous chemicals has a negative effect for the ecology of our environment.

As a result, green synthesis of metal oxide nanoparticles and nanocomposite has received special attention due to a cheaper and environmentally friendly method. This green method of synthesis refers to the formation of nanoparticle structures which are capped by organic materials from living organisms or plants [19]. Here in, ZnO/CuO nanocomposites were synthesized using *Musa acuminata* peel extract as stabilizing and capping agents for degradation of organic dye.

1.2. Statement of the problem

Organic pollutants in wastewater are one of the hazardous and non-degradable due to their physicochemical composition [20]. Among the organic pollutants organic dyes are discharged with trace amount from leather, paper, food, and cosmetics industries to the environment. They are highly hazardous in the environment and are potentially toxic toward humans, animals and plants [21]. Therefore, remediation to remove these contaminants efficiently from the industrial effluent and thus from the environment for the sake of human and environmental well-being has to be sought. With this in mind, the application of metal oxide nanomaterials for photo-degradation of organic pollutant in wastewater becomes the main research area.

ZnO NPs is a good candidate for photo-catalytic pollutant removal because of its low cost, high photosensitivity, and nontoxic nature. However, the rapid charge carrier recombination and wide band gap of ZnO limit its photo-catalytic efficiency. One of the best approaches to overcome these issues is coupling ZnO NPs with another semiconductor such as CuO NPs. As combining ZnO with CuO could extend the activation range into the visible light region resulting in more efficient separation of electron–hole pairs, this may enhance the photocatalytic efficiency not only in the UV region but also in the visible light region [22].

Regarding the synthesis, several chemical synthesis techniques have been used for the synthesis of ZnO/CuO nanocomposite which are not environment friendly. However green synthesis process has been accepted as a promising technique to prevail the limitations accompanied with chemical methods. Furthermore, green synthesis of ZnO/CuO nanocomposite has been rarely studied. So, further study of the plant mediated synthesis of this nanocomposite is important.

Here in, *Musa acuminata* peel is used for the synthesis of ZnO/CuO nanocomposite. This plant constitute different bioactive compounds like polyphenols which can act as reductants and amines and carboxyl groups that help to stabilize, in favour of converting metal compounds into specific NPs [23]

1.3. Objectives of the study

1.3.1. General objective

To synthesize, characterize and evaluate the photo-catalytic performance of ZnO/CuO nanocomposite.

1.3.2. Specific objectives

- To extract bioactive compound from *Musa acuminata* peel,
- To synthesis CuO NPs, ZnO NPs and ZnO/CuO nanocomposite materials by green sol gel route,
- To characterize the synthesized ZnO, CuO, and ZnO/CuO nanoparticles and nanocomposite using UV-DRS, XRD, TGA/DTA and SEM characterization techniques,
- To evaluate the photocatalytic degradation performance of the synthesized nanoparticles and nanocomposite using methylene blue dye from synthetic water,

- To optimize precursor salt of ZnO, ZnO with CuO as well as to optimize the working parameters such as pH of medium, catalyst loading and pollutant concentrations for better photo-catalysis performance.

1.3.3. The scope of the study

The scope of this study was limited to synthesis of ZnO and CuO NPs and ZnO/CuO nanocomposite using *Musa acuminata* peel extract. Characterizations of the synthesized nanoparticles and nanocomposite using TGA-DTA, UV-DRS, XRD, FTIR, and SEM and evaluation of the photocatalytic degradation of methylene blue using the synthesized nanoparticles and nanocomposites.

1.3.4. Significance of the study

The finding of this study will redound to the benefit of society considering that pure water is verry important for healthy life. The considerable increase of organic dyes in wastewater is a great challenge worldwide. Organic dyes are difficult to be removed by conventional water treatment methods because of the presence of multiple aromatic rings, which are difficult to degrade by conventional methods. The greater increase of organic dyes in wastewater justifies the need for effective wastewater treatment (i.e. AOPs). This study provides the most acceptable method for treatment of water polluted by industrial textile dyes such as MB. Finally, other researchers also can be benefited from these research as they get an idea or gap from it.

2. Literature review

2.1. Water pollution

Water pollution is the presence of excessive amounts of a hazard (pollutants) in water in such a way that it is no long suitable for drinking, bathing, cooking or other use [24].Contaminants released from industries and agricultural activity have become the main source, which affects most of the water bodies in the ecological system [25]. Organic dyes are one of the leading groups of pollutants released into wastewaters from textile and other industrial processes. About 10–20% of total dye products in the world is lost in textile wastes during the manufacturing process and released as effluents into the green environment [26]. Many industries use dyes extensively for various operations such as textile, paper, plastic, leather, tanning, etc. These industries discharge mixing of pollutants in a different process.

2.1. 1. Wastewater treatment methods

2.1.1.1. Conventional wastewater treatment methods

A large number of conservative treatment processes have been employed in various industrial wastewaters such as chemical, biological, food, pharmaceutical, pulp and paper, dye processing, and textile wastes [27]. Conventional wastewater treatment consists of a combination of physical, chemical, and biological processes and operations to remove solids, organic matter and, sometimes, nutrients from wastewater. However, these conventional treatment processes are not successful for organic dyes and the high salinity of wastewater containing dyes because of the recalcitrant nature of synthetic dyes [28]. Furthermore, traditional physical techniques such as adsorption on activated carbon, ultrafiltration, reverse osmosis, coagulation by chemical agents, ion exchange on synthetic adsorbent resins, etc., have been used for the removal of dye pollutants [29]. These methods are successful only in transferring organic compounds from water to another phase, thus creating secondary pollution which requires further treatment of solid wastes and regeneration of the adsorbent which makes the process costlier. Therefore, substantial attention has been focused on complete oxidation of organic compounds to harmless products such as CO_2 and H_2O by the advanced oxidation process (AOP) and appears as one of the most confidential technologies.

2.1.1.2. Advanced oxidation process (AOP) for wastewater treatment

The use of techniques based on chemical oxidation for the treatment of water bodies contaminated by domestic and industrial effluents, which are rich in toxic organic compounds, has been proposed in order to reduce environmental pollution and to enable the recycling of water resources [30].In the last decades, researchers who have studied alternative treatments to toxic contaminants have concluded that advanced oxidative processes (AOPs) are highly efficient due to the high number of contaminants that can be oxidized.

These processes comprise a number of methods, which include ozonation, photocatalysis, electrochemical oxidation and the Fenton reaction. These treatment processes consist in the generation of hydroxyl radicals ($OH^{\bullet}$) that are highly reactive, non-selective and promote the mineralization of organic contaminants, generating CO_2, H_2O and inorganics, or producing either harmless or biodegradable products [31].

2.2. Heterogeneous photo-catalysis

Photocatalysis is one of the advanced oxidative processes whose principle involves the activation of a catalyst through sunlight or artificial light. The process consists of the absorption of photons with energy higher than the band gap energy of the semiconductor that generates electron/hole (e^-/h^+) pairs in the conduction (CB) and valance bands (VB) of the semiconductor. The photogenerated e^-/h^+ pairs will take part in the redox reactions to produce the final products [32].

2.2.1. Mechanism of Heterogeneous photo-catalysis

There are four major steps that takes place during photo-catalytic reactions after the absorption of light by a photo-catalyst: (i) formation of the charge carriers over the VB and CB as the incidence of light with the same or higher energy than the energy gap (Eg) of the employed semiconductor excites electrons from the VB to the CB, leaving positive holes in the VB, thus forming e^-/h^+ pairs, (ii) recombination of the photo-generated e^-/h^+ pairs since the photo induced e^-/h^+ pairs are not energetically stable and some of them undergo recombination course and neutralize each other , (iii) trapping of the e^-/h^+ pairs in red-ox reactions in which the photo induced holes and

electrons transfer to surface of the photo-catalyst and react with the adsorbed species on the surface and finally (iv) the main photo-catalytic reactions such as degradation of the pollutant by reduction and oxidation reactions over the CB and VB of the photo-catalyst take place depending on the type of the photo-catalytic processes [33]. A simplified schematic of the photo- catalytic process is illustrated in Figure 1.

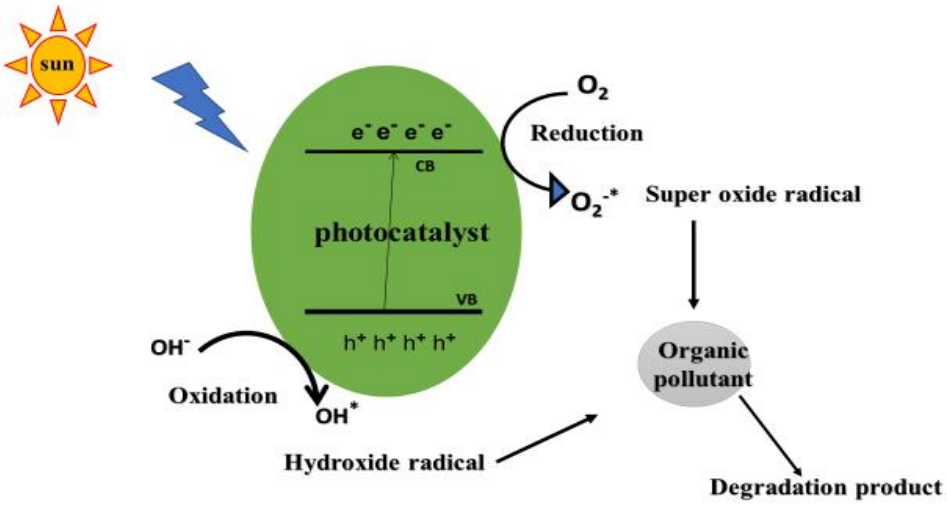

Figure 1 Schematic representation of semiconductor photo-catalytic mechanism

2.2.1.1. Oxidation Mechanism

In oxidation mechanism water molecules on the photo-catalyst surface is oxidized by hole (h^+) created in the VB due to the electrons (e^-) shift to the CB as a result of light irradiation, thus making way for the formation of hydroxyl radicals ($OH^{-\cdot}$) which have strong oxidative decomposing power. Subsequently, these $OH^{-\cdot}$ react with organic matter present in the dyes. Finally the organic matter decomposes ultimately in to carbon dioxide and water [34]. Under such circumstances, organic compounds can react straightly with the positive holes, resulting in oxidative decomposition. The complete oxidation processes are shown in Figur.2

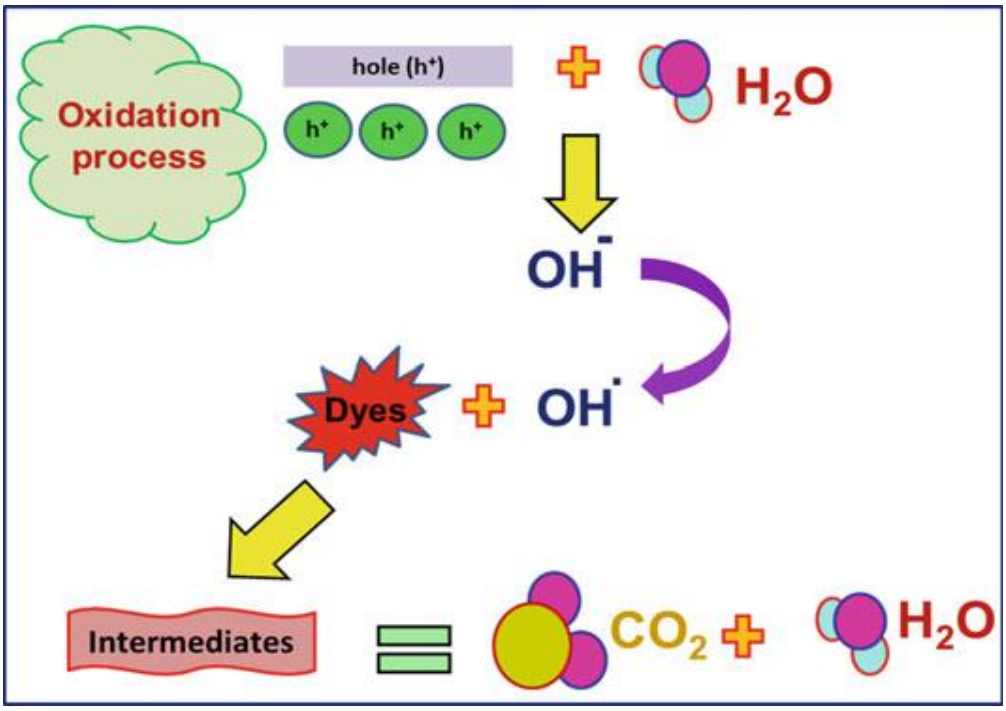

Figure 2 Schematic representation of oxidation mechanism [34].

2.2.1.2. Reduction Mechanism

In reduction mechanism CB electrons react with dissolved oxygen species to form superoxide anions ($O_2^{-\cdot}$). These superoxide anions attach to the intermediate products in the oxidative reaction, forming peroxide or changing to hydrogen peroxide and then to water. The reduction is likely to occur more easily in organic matter than in water. Therefore, the higher concentration of organic matter tends to increase the number of positive holes. This reduces the carrier recombination and enhances the photo-catalytic activity [34]. Figure.3 represents the reduction process, the reduction of oxygen contained in the air occurs as a pairing reaction.

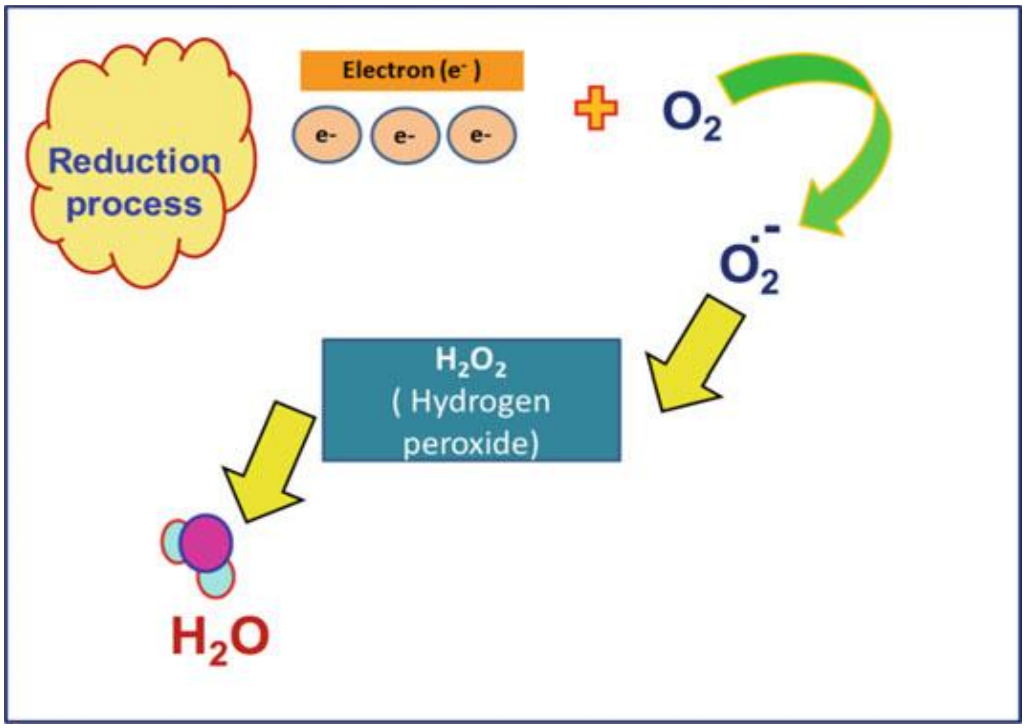

Figure 3 Schematic representation of reduction mechanism [34].

2.2.2. Factors affecting photo-catalysis

Parameters such as structure, shape, size, and surface area of the catalyst, reaction temperature, pH, light intensity, amount of catalyst and concentration of wastewater can affect rate of photo degradation of an organic compound by photo-catalyst [35].

2.2.2.1. Crystal Structure, Shape, Size, and Surface Area of Catalyst

The structure of catalyst plays a key role in achieving superior photo-catalytic activity. For instance among three phase of TiO_2 (anatase, rutile, and brookite), anatase is the most sensitive and attractive phase for photocatalytic activity due to its stability, the position of the conduction band, the higher degree of hydroxylation, and adsorption power [36].Furthermore morphology also acts as a potential factor that influences the final degradation efficiency. Various studies have been attempted at the production of ZnO with different nanostructures as zero-dimensional (0D), one-dimensional (1D), two-dimensional (2D) and three-dimensional (3D)[37]. Compared with 0D and 1D ZnO nanostructures, ZnO nanosheets(2D) are more suitable for the construction of high-performance photocatalysts, because they have two-dimensional characteristics, high specific

surface area to expose abundant active sites and short bulk diffusion length to improve electronic transport efficiency [38]. Jang et al reported that the large specific surface area and polar faces possessed by 2D ZnO make ZnO nanosheets superior candidates for photocatalysis [39]. The large specific surface area of ZnO enables more contaminants to be adsorbed onto its active surface and thus lead to more pollutants being attacked by hydroxyl radicals. The chain reaction that occurs at the surface enhances the degradation rate of the contaminants to produce non-toxic products.

2.2.2.2. Effect of Reaction Temperature

A number of studies have been demonstrated to stud the dependence of photo-catalytic activity on reaction temperature .Salama et al. [40] demonstrate that photo-degradation process is very sensible to changes in temperature. The result of their experiments indicated that, the full degradation was achieved at the lowest dye concentration, the lowest pH and at a high temperature. Yanjun X et al. [41]also demonstrate as the photo-catalytic reaction temperature affects the degradation efficiency of the photo-catalyst by utilizing as synthesized CuS-CdS/TiO_2nanoboots for the degradation of Toluene at 20, 30, 40 and 50ºc reaction temperature. Their results show that photo-catalytic efficiency of the photo-catalyst increase with the temperature but, decrease after 40ºC.

2.2.2.3. Effect of pH

The photo-catalytic degradation is mainly dependent on the pH value due to its effect on the catalyst charge, aggregates' size, and valance and conductance bonds position. Kazeminezhad et al.[42] reported the effect of solution pH on photo-catalytic activity of ZnO NPs. The effect of solution pH on activity of ZnO NPs was investigated by repeating the experiments at three pH (4, 8 and 11) for RB, MB and BG dyes. The results demonstrated that the adsorption of the dyes onto ZnO NPs surface is strongly dependent on pH of the reaction solution and is an important step in photo-catalytic degradation. It was observed that, RB dye degraded more rapidly at pH = 4 and 8 in comparison with pH = 11 with no adsorption onto nanoparticles surface. For MB and BG high decomposition rate occur at pH = 11 and pH = 8, respectively, with the highest optimum adsorption.

2.2.2.4. Effect of Light Intensity

The degradation rate of photo-catalytic reaction mostly depends upon the light intensity. The quanta of light absorbed by any photo-catalyst or reactant are given by the quantum yield which is the ratio of the rate of reaction to the rate of absorption of radiation. The result of photo-catalytic reaction responses varied under different wavelengths of the light source [43].

2.2.2.5. Effect of Amount of Catalyst

The amount of catalyst also influences the efficiency of photo-catalytic degradation. If there is an increase in the quantity of catalyst, the number of active sites on the semiconductor surface increases moreover, which in turn produces number of $OH^{-\cdot}$ and ($O_2^{-\cdot}$ radicals [28]. As a result, the photo-catalytic degradation rate is increased. However, as the catalyst loading is improved beyond an optimum concentration, the degradation rate is unfavorable because there will be decrease in the light penetration depth into the solution and consequently diminishing of light scattering occurs [44].

2.2.2.6. Concentration of Pollutants

The photo-catalytic degradation rate of a certain dye or pollutant depends on its concentration, nature and on the presence of other existing compounds in the water matrix. Salama et al .[40] study the effect of the dye's concentration on the photo-degradation efficiency for MB and IC (indigo carmine) using composite nanofibers under UV irradiation. The degradation efficiencies were studied at 10, 30, and 50 ppm. The result indicated that the degradation efficiencies were, respectively,100, 80, and 70% for MB and 100, 90 and 80% for IC. High concentration of the dye activated the photo-catalytic process, but reduced the degradation rate. This result is due to the saturated surface of the catalyst which is caused by the high concentration of the dye. In this regard, the photo-catalytic degradation reaction will be deactivated.

2.3. ZnO based photocatalysis

ZnO NPs is considered as an adaptable semiconductor photo-catalyst for the photo-oxidation of organic pollutants [45]. It is an eco-friendly material as it is congruent with living organisms providing a broad range of daily applications without any risky effect on human health and environment. Along with this, it has large efficiency for removal and complete degradation of

environmental pollutants. Several researchers have reported the use of ZnO as a photocatalyst in degrading organic pollutants. For instant Nandini et al.[46] synthesis ZnO nanorods having uniform size using hydrothermal method and show 65% MB dye degradation within 50 min under solar light irradiations. Similarly *Mohd* et al. [47] synthesize ZnO-NPs via coprecipitation technique by treating zinc nitrate solution with sodium hydroxide in the presence of leaf extract. The synthesized ZnO-NPs were tested for the decolorization of MB under visible and UV irradiation giving an efficiency of 19.8 and 88.2 % respectively. Another researchers Perumal et al.[48] synthesis hairy shaped ZnO photocatalyst by uratolytic bacteria mediated synthesis for degradation of dye viz MB, MO, Rho-B and fresh textile effluents. The hairy structured ZnO facilitates photocatalytic decolorization under the UV-light. After all, the rapid charge carrier recombination and wide band gap of ZnO limit its photo-catalytic efficiency.

2.3.1. Limitation of ZnO NPs as photo-catalyst

ZnO as photo-catalyst has a number of problems in use: (i) the wide band gap energy of ZnO does not help for absorption of visible light, so it can only get benefit from a small fraction of the solar beam that reaches the earth (3–5%), (ii) the high rate for recombination of the photo induced charge carriers that stops them from reaching to surface, leading to retardation of the chemical reactions that take place at the semiconductor/liquid interface; and (iii) ZnO has high photo corrosion when subjected to the irradiation. Therefore, pure ZnO does not have acceptable activity under solar energy [49]. In light of these, extensive researches have focused on improving photo-catalytic activity of ZnO NPs. To overcome this drawback, researchers developed several methods, such as doping of metal/nonmetal atoms, depositing noble metals, and coupling with other semiconductors or carbon materials [22].

2.3.2. Techniques for enhancing photo-catalytic activity of ZnO

In principle, photo-catalytic activity will be enhanced if the absorption of light is higher or if the recombination losses for photo-generated charge carriers are lower. There are different strategies to enhance the photo-catalytic activity of ZnO NPs. Among them doping with metal, nonmetal and coupling of ZnO NPs with another semiconductor are prominent one [50].

2.3.2.1. Doping

Doping of photocatalysts with non-metals, transition-metals, noble metals or lanthanide ions are the methods employed for retarding the fast charge recombination and enabling visible light absorption by creating defect states in the band gap [51].

2.3.2.1.1. Metal doped ZnO NPs

Metal doping of ZnO can improve the photo-activity of catalysts by increasing the trapping site of the photo-induced charge carriers and thus decrease the recombination rate of photo-induced electron-hole pairs [52]. In order to decrease the band gap energy of photo-catalysts, metal dopants such as Ce, Nd, Cu and Al have been used in applications in dye degradation and gas sensor [53]. Yun et al. [54] have shown that higher loads of organic compounds could be adsorbed on Al doped ZnO compared to pure ZnO based on the high light harvesting efficiency. Zhu et al.[52] also reported that the incorporation of metal ions such as Fe^{3+}, can contribute to more oxygen defects on ZnO along with an increase in the charge density of ZnO, which subsequently can induce higher performance of the nanostructure.

2.3.2.1.2. Non-metal doped ZnO NPs

In the nonmetal doping case, incorporation of dopant leads to the creation of local states inside the band gap and the absorption on set of semiconductor can be extended from the UV to visible-light region through band gap narrowing [55]. ZnO doping with nonmetals, such as carbon (C), nitrogen (N), and sulfur (S) can lead to the formation of intermediate energy levels and extend the valence band, which causes visible-light photo-catalytic activity [56]. Shelja et al. [57] synthesized N-ZnO/C-dots nanoflowers for Mg degradation under visible light irradiation. The photocatalytic efficiency of N-ZnO/C is (85%) which is higher than ZnO (65%). Hanggara et al.[58] synthesize visible light active N doped ZnO through a combustion reaction. The N doped ZnO show 89.3% of MB degradation with initial concentration of 10 mg/L within1.5 h under visible light.

Weilai et al [56] also studies C,N and S doped ZnO and investigate the electronic structures, optical properties and effective masses of charge carriers by first-principle density functional theory calculation. The calculation of the effective masses show that ZnO typically possess light electrons and heavy holes, confirming its intrinsic character of n-type semiconductor, while N, C

and S doping can generally render electrons lighter and holes heavier, resulting in slower recombination rate of photogenerated electron–hole pairs.

2.3.2.2. Coupling with other semiconductors

The coupling of other semiconductors to form heterojunctions with ZnO is also interesting because varying interfacial interactions provide new properties, which do not belong to any individual nanomaterial [59]. A prolonged carrier lifetime and an enhancing interfacial charge transfer can be obtained from such heterostructures [60].

The literature is replete with the studies on various ZnO-based photocatalysts through coupling with small band gap semiconductors. For example Rui et al. [61] fabricate TiO_2-ZnO composite photocatalysts by simple hydrothermal method and the photocatalytic property of as-prepared samples were analyzed by the photo degradation of rhodamine B water solutions under visible light irradiation. Lee et al. [62] also synthesized ZnSe/ZnO heterostructures through simple solution-based reactions. The ZnSe/ZnO heterostructures possessed higher activity than that of pure ZnO in visible-light photodegradation of orange-II. Table 1 illustrate some studies on ZnO-based photocatalysts.

Table 1 Recent studies about the application of narrow band gap materials coupled with ZnO**.**

Narrow Eg S.conductr	Band gap	Photo-catalyst	Synthesis method	Photo-catalytic efficiency	Ref
Cu_2O	2.17 eV	ZnO/Cu_2O nanostructure	Hydrothermal	100% in 380 min	[63]
In_2O_3	2.8 Ev	In_2O_3/ZnO heterostructure	Hydrothermal	98% in 6 h	[64]
AgCl	3.0 eV	AgCl–ZnO nanocomposite	Refluxing	100% in 330 min	[65]
V_3O_4	2.9 eV	ZnO/V_3O_4 nanostructure	Hydrothermal	97% in 16 min	[66]
Mn_2O_3	2.2 eV	ZnO/g–Mn_2O_3	Thermal decomposition	95% for MB in 210 min	[67]

$ZnFe_2O_4$	1.9 eV	nFe_2O_4/ZnO multi-porous nanotube	Electrospinning–calcinations	99% in 150 min	[68]
$BiVO_4$	2.4 Ev	$BiVO_4$/ZnO nanosheet	Hydrothermal	100% in120 min	[69]

2.4. Coupling of ZnO with CuO

2.4.1. CuO NPs

Cupric oxide (CuO) is a p-type semiconductor with a narrow band gap (Eg 1.2 eV) [70]. Outstanding characteristics such as thermal stability, optical properties and electrical conductivity of copper oxide inspired the researcher to work on this material for photocatalytic activity and electrical conductivity [70]. Despite the attractive features of CuO for photo-catalytic processes under visible light, the performance of CuO-based photo-catalysts is far below expectation as a result of the recombination of photo-generated electron-hole pairs [71]. It is extremely desirable to decrease the rate of recombination of photogenerated carriers. Therefore, CuO nanostructures could be coupled with other semiconductors such as ZnO which increases the electron hole separation leading to the enhancement in photocatalytic activity.

2.4.2. ZnO/CuO nanocomposite

Among various ZnO coupled semiconductors, ZnO/CuO is considered as a promising mixed metal oxide semiconductor photocatalyst because of its photo-catalytic activity, magnetic properties and gas sensing ability[72].

As an important p-type narrow band gap semiconductor, CuO NPs has been applied to ZnO to form ZnO/CuO hetero-junctions [73] which give rise to maximum photo- catalytic activity by transferring the charge carriers from CuO to ZnO (Figure 4). This transfer decrease recombination rate of photoexcited e^-/h^+ pairs. Moreover, the combination of CuO and ZnO enhances the response to visible light and increases the photo-catalytic activity in the common visible light range [74].

However, few researches have investigated the effect of ZnO/CuO composite, which has great potential in degrading organic pollutants due to differential band energies of ZnO (3.4 eV) and CuO (1.2 eV), which cover the UV and visible light region. For example, Shreyasi et al. [75] have

synthesized ZnO/CuO nanocomposites by solution process and investigated the photo-catalytic decomposition of methyl orange and rhodamine B. The enhanced photocatalytic activity was observed for ZnO/CuO compared to pure ZnO and CuO. Jianyu et al. [76] have reported a 3D hetero-hierarchical device consisted of 2D CuO nanosheets and 1D ZnO nanorods. The photocatalytic reduction of aqueous Cr (IV) was investigated and shows the enhanced photocatalytic activity. Benxia et al.[77] studied the photocatalytic activity of pure and ZnO/CuO nanocomposites. They have reported that ZnO/CuO nanocomposites show maximum activity compared to pure ZnO and CuO. This is attributed to the extended photo-responding range and increased charge separation rate in ZnO/CuO composites.

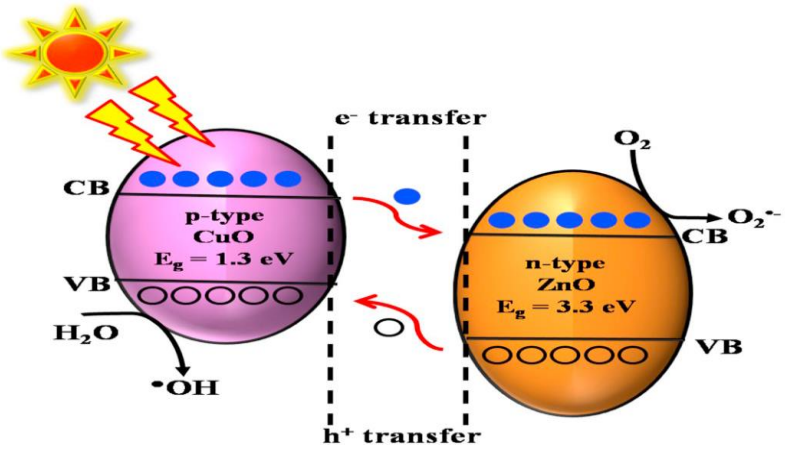

Figure 4 Schematic illustration of the formation of charge carriers (e^- and h^+) and photo-catalytic degradation of pollutant on the ZnO nanostructured surface [78].

2.5. Synthesis of ZnO/CuO nanocomposite

There are many reports on ZnO/CuO heterostructures of varies compositions and morphologies synthesized using different synthesis methods. Li and Wang [76] reported ZnO/CuO nanocomposite synthesis by co-precipitation method that result the improvement of ZnO and CuO photo-catalysis performance. Muzakki et al. [79] also synthesized monoclinic CuO-doped hexagonal wurtzite ZnO-shaped CuO-ZnO nanocomposites with sol gel technique for effective degradation of textile dye in aqueous solution. Mansournia and Ghader fabricated CuO@ZnO core-shell nanocomposite using a simple two-step hydrothermal method with the enhancement of catalytic activity of ZnO in photo-degradation of MB under UV irradiation [80].

Several methods are used for metal oxide nanocomposite synthesis such as hydrothermal [15], electrochemistry [16], wet chemical [17], microwave method [81]cop-precipitation, sol–gel, wet impregnation, and thermal decomposition [77, 82]. However, the classical method to synthesis of metal oxide nanoparticles using hazardous chemicals has a negative effect for the environment.

2.5.1. Green synthesis of ZnO/CuO nanocomposite

Green synthesis of ZnO/CuO nanocomposite is very advantageous because it is relatively simple and environmentally safe [83]. These methods utilize natural products, which are the key ingredients in green synthesis of nanocomposite [84] and by utilizing these readily available and renewable sources, the production of nanocomposite are no longer limited to costly and dangerous methods.

For the green synthesis of nanocomposite natural reagents such as microorganisms, fruits, marine algae, sugars, plant parts (roots, seed, leaf, steam and latex) are used [85]. Plants is more preferable due to the coexistence of different bio-molecules such as bioactive flavonoids, polyphone, phenolic acids, terpenoids, carbohydrate, fats, amino acids, gum, polysaccharides, alkaloids, alcoholic compounds, which are playing a significant role in reducing the metallic ions first and then acting as a capping or chelating agent [85]. In addition to these various fruit peel extracts are the subject of great interest as they possess similar properties to plant extracts such as being rich in bio-components that play a major role in the biological synthesis of nanoparticles and are also easily obtainable [86].

Mohammadi et al. [87] fabricated ZnO NPs and ZnO/CuO nanocomposites using green method for efficient antibacterial activity. Another study by Yulizar et al. [88] used green method to synthesize ZnO/CuO nanocomposite using Theobroma cacao seed bark extract (TBE) to decrease a high band gap energy of ZnO. Researches done on green synthesis of ZnO, CuO and ZnO-CuO nanocomposite are indicated in Table 2. These are the only researches that use green route to synthesis ZnO/CuO nanocomposite. For that reason, further studies are required on green synthesis of ZnO/CuO nanocomposite. Furthermore, green synthesis of ZnO/CuO nanocomposite using *Musa acuminata* Peel extract has not been ever investigated yet in the previous research.

Table 2 Green synthesis ZnO, CuO and ZnO-CuO nanocomposite.

Materials	Precursor	Methods	Stabilizing and capping agent	Particle size result
ZnO NPs [89]	$Zn(NO_3)_2$	Green synthesis	*Imperata cylindrical*	11.9 nm
ZnO NPs [90]	$Zn(NO_3)_2$	Green synthesis	*Moringaoleifera*	12.27–30.51 nm
ZnO NPs [91]	$Zn(NO_3)_2$	Green synthesis	*Vitextrifolia*	15–46 nm
CuO NPs [92]	$CuSO_4$	Green synthesis	*Callistemon viminalis*	3.8–42.4 nm
CuO NPs [93]	$Cu(NO_3)_2$	Green synthesis	*Calotropisgigantean*	20 nm
CuO NPs [94]	$CuCl_2$	Green synthesis	*Theobroma cacao*	40 nm
CuO–ZnO core shell Nanocomposite [95]	ZnO NPs, $CuCl_2$	Green synthesis	*Melissa officinalis*	10–20 nm
CuO–ZnO Nanocomposite [88]	$Zn(NO_3)_2$ $Cu(NO_3)_2$	Green synthesis	Theobroma cacao seed bark	20–50 nm
ZnO/CuO nanocomposite (this work)	$Cu(NO_3)_2$ $Zn(CH_3COO)_2$	Green synthesis	*Musa acuminate* peel	20-23 m

2.6. *Musa acuminate* (banana) peel

Musa acuminata (banana) is worldwide consumed and after the consumption of the pulp, the peels are usually discarded [96]. Banana peel is known to be rich in phytochemical compounds, especially antioxidants and phenolic compounds which can be used in medical field against cancer and heart disease since it has good antioxidants with various types of antioxidant compounds, such as gallocatechin and dopamine [97]. The presence of hydroxyl and carbonyl group of the pectin has increased the absorption capacity and the organic compound of banana peel. This statement has been proven by Kamel et. al [23]. Based on their study, the functional groups that have been found were O-H stretching, C-H stretching of alkane, C-O stretching of carboxylic acids, C-C bond of diene, N-H deformation of amine and the functional group that attributed to ester, polysaccharide or protein.

In today study *Musa acuminata* Peel extract is suggested for the synthesis of ZnO/CuO nanocomposite. This plant constitute different bioactive compounds like polyphenols which can act as reductants and amines and carboxyl groups that help stabilize, in favor of converting metal compounds into specific NPs [23].

3. Materials and Methods

3.1. Materials

In this research, zinc (II) acetate dihydrate [Zn $(CH_3\ COO)_2 \cdot 2H_2O$] (99% pure) and copper (II) nitrate trihydrate [Cu $(NO_3)_2.3H_2O$] (99% pure) were used as precursors for the synthesis of ZnO and CuO NPs, respectively. Sodium hydroxide (NaOH) and ethanol (97% pure) were used as precipitating agent and for washing purpose, respectively. Distilled water was used as the synthesis medium. All chemical reagents were purchased from Merck and Aldrich Chemical Companies with analytical grads.

3.2. Sample collection and Preparation of *Musa acuminata* peel extract

Musa acuminata peels were obtained from local fruit market located in Adama city, East Shoa Zone, Oromia Regional state, Ethiopia. The collected peels were washed with distilled water and dried in an oven at 60^{o}C for 24 hrs. and then ground into a moderately fine powder. Afterwards, 30 g of the dried peel was dissolved in 300 ml of distilled water and stirred for 1hr at 50^{o}C. Finally, the boiled sample were filtered using a filter paper and the solution was used as a plant extract [98].

3.3. Synthesis of ZnO NPs using aqueous extract of *Musa acuminata* peel

The synthesis of the ZnO NPs with green sol gel method was carried out by dissolving 4.04 g of zinc (II) acetate dihydrate [Zn $(CH_3\ COO)_2 \cdot 2H_2O$] in 66ml of distilled water (0.27M) followed by drop wise addition of this solution to 33 mL of aqueous extract of the banana peel with continues stirring. After 30 min an aqueous solution of NaOH (1 M) was added drop wise into the solution under stirring to adjust pH to 12. Then the solution was stirred for 3 hrs. The mixture was kept for 24 hrs. to form a gel and washed with distilled water and ethanol several times. Then, the gel was dried in an oven at 60°C and calcined at 500°C for 2 hours to obtain the ZnO NPs [87]. The steps were repeated for 0.36 M and 0.55 M of zinc acetate for the same volume of plant extract. For

simplification they labeled as 1:1 ,1:2, and 1:3 indicating 0.27 M, 0.36 M and 0.55 M of zinc acetate for the same volume of plant extract respectively.

The same procedure was carried out for green synthesis of CuO by dissolving 4.56 g of copper (II) nitrate trihydrate [Cu $(NO_3)_2.3H_2O$] in 66 ml distilled water.

3.4. Synthesis of ZnO/CuO nanocomposite using the aqueous extract of *Musa acuminata* peel

ZnO/CuO nanocomposite was synthesized by the green sol gel method. In the case of the ZnO/CuO (10%) nanocomposite, 2.29 g of zinc (II) acetate dihydrate [Zn $(CH_3\ COO)_2{\cdot}2H_2O$] and 0.337 g of copper (II) nitrate trihydrate [Cu $(NO_3)_2.3H_2O$] were each dissolved in 40 ml of distilled water in different beaker. Then 40 ml zinc acetate solution was added drop by drop to 33 mL of aqueous extract of the peel with continues stirring. After 30 min, 40 ml copper nitrate solution was added drop by drop to the above solution. After 30 min of stirring, the pH of the solution was adjusted to 12 by drop wise addition of an aqueous solution of NaOH (1M). After continuous stirring for 3 hrs, the solution was kept for 24 hours to form a gel and washed with distilled water and ethanol several times. Then, the gel was dried in an oven at 60 °C and calcined at 500 °C for 2 hrs to obtain the ZnO/CuO nanocomposite. For synthesis of the ZnO/CuO with (15%), 20% and (25%) nanocomposite, the amounts of copper nitrate used were 0.53 g , 0.76 g and 1.01 g, respectively for the same gram of zinc acetate [88]. For simplification they labeled as ZC10, ZC15, ZC20, and ZC25, for 10% ZnO/CuO, 15% ZnO/CuO, 20% ZnO/CuO and 25% ZnO/CuO respectively.

3.5. Characterization of the as synthesized nanomaterials

The crystal structures of the as synthesized ZnO NPs, CuO NPs and ZnO/CuO nanocomposite were characterized using X-ray diffraction (XRD-700 Shimadzu Co., Japan, λ_{CuK1} = 0.15406 nm, tube voltage 40 kV, current 30 Ma). The formation of NPs, nanocomposites and the absence of any other functional groups from the precursors were confirmed using Fourier Transform Infrared Spectroscopy (FTIR) (FT/IR-6600 Co, Jasco). The morphology of the catalysts prepared was done by a scanning electron microscopy (SEM, JSM 6000). TGA studies of the nanoparticles were carried out using a TGA/DTA apparatus (DTG-60H Shimadzu Co., South Korea). UV- Vis DRS

spectrometer (UV-3600 Shimadzu Co., Japan) was used to record the UV-visible diffuse reflectance spectra in the range of 220–800 nm using $BaSO_4$ as a reference standard material.

3.6. Photocatalyst experiment

The photocatalytic activities of the synthesized samples were evaluated by the degradation of an aqueous solution of different concentration of methylene blue (MB). The reactions were carried out in a discontinuous mechanical stirring photoreactor with 400 W Osram lamp. The lamp was placed inside a quartz container with two cabins: one contained the lamp and the other makes water to pass into a recirculation channel for temperature control. Before irradiation, 35 mg of catalyst were added to the dye solution (0.22 L) and sonicated in the dark for 30 min to reach the adsorption equilibrium. Afterwards, the visible lamp was switched on, and aliquots of the aqueous suspension were collected from the reactor every 15 min and then centrifuged to remove the photocatalyst particles. The concentrations of MB were determined from absorbance from UV–visible spectrophotometer at 664 nm. Finally, the photocatalytic degradation efficiencies of the samples were calculated using Eq.1 [99].

$$\text{Degradation } (\%) = \left(\frac{A_0 - A_t}{A_0}\right) * 100 \quad (1)$$

Where, A_0 is the initial absorbance of dye solution, and A_t is the dye solution absorbance at a certain reaction time.

4. Results and discussion

4.1. Thermal analysis

The thermogravimetric analysis and differential thermal analysis (TGA/DTA) curves of the as-prepared ZnO NPs and CuO NPs are displayed in figure 5. Figure (5a) shows TGA/DTA curve for the ZnO sample with three main stages of weight loss. The three endothermic peaks indicated by bend Ed_1, Ed_2 and Ed_3 in DTA curve with a first weight loss of 5.76% at 80°C and from 140 - 155°C in TGA curve can be associated to removal of surface water and decomposition of chemically bound groups respectively. The second weight loss (6.4%) in the range of 175-380°C, accompanied by one endothermic and one strong exothermic peak indicated by bend Ed_4 and Ex in DTA curve, may be attributed to decomposition of organic compounds of peel extract [100].

Furthermore, thermal stability of ZnO sample was achieved after third mass loss of 0.134%, between the temperatures of 380 and 450 °C. These loss can be attributed to the decomposition of the residual precursors and removal of gases such as CO_2 in air with formation of ZnO NPs [99]. After 450 °C, there was no negligible weight loss indicating impurities are removed and the ZnO nanoparticles are thermally stable.

Figure 5 (b) shows the TGA/DTA curve for CuO NPs. The first endothermic peak (Ed_1) between 80^{o}C and 100^{o}C in DTA curve (14% weight loss from TGA curve) can be associated with dehydration of water from the sample. In further heating of these samples between the temperature of 200^{o}C and 350^{o}C, the sample showed mass loss of 22.9% with strong exothermic and weak endothermic peaks (Ex and Ed2) in DTA curve. This can be related to the decomposition of the organic compounds from the fruit extract attached to the surface of the CuO samples [100]. Furthermore, thermal stability of CuO sample was obtained after mass loss of 1.9%, with weak

endothermic peaks between the temperatures of 350 and 450 °C. These mass losses can be attributed to the decomposition of Cu salt to form CuO.

The TGA/DTA analysis of ZnO and CuO implies that calcination temperatures between 450^0C and 500^0C would be a satisfactory temperature for the precursor decomposition to acquire the CuO NPs, ZnO NPs and ZnO/CuO nanocomposites.

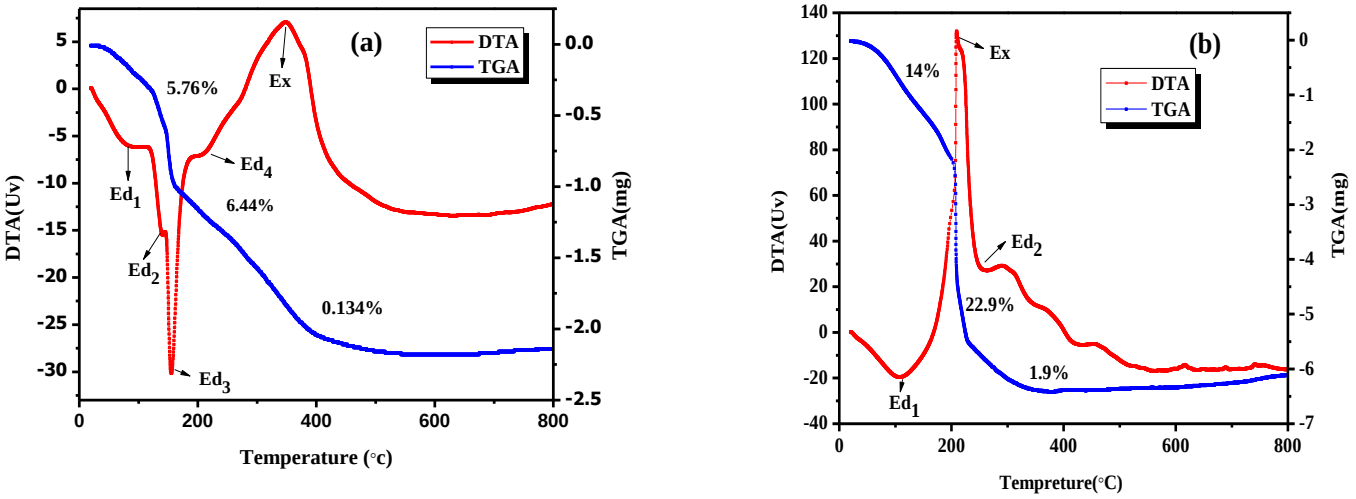

Figure 5**.** GTA-DTA graph of the as synthesized ZnO NPs (a) and CuO NPs(b) with fruit peel extract.

4.2. XRD Analysis

The crystalline structure and phase purity of the samples were characterized by XRD. Figure 6a comprise the XRD patterns of the as synthesized ZnO with different precursor concentration and BP extract (1:1,1:2 and 1:3). According to XRD patterns, the synthesized 1:1,1:2 and 1:3 samples showed the same pattern as standard ZnO with the same plane value. The diffraction peaks located at (1 0 0), (0 0 2), (1 0 1), (1 0 2), (1 1 0), (103), (100), (112), (20 1), (004), and (202) at 2θ values of 31.83 º, 34.49 º, 36.32 º, 47.60 º, 56.67 º, 63.52 º, 67.60 º, 68.03 º, and 69.15º, respectively, were consistent with standard of JCPDS Card at references code (00-036-1451) [101]. This indicates that the peaks are belongs to hexagonal wurtzite structure of ZnO.

In addition to these, a sharp and narrow diffraction peak for each sample were observed which is due to the reduction of zinc ions by organic compound present in the BP extract and stabilization of resultant nanoparticles [96]. According to Elumalai and Velmurugan [102], the sharp and the narrow image of the diffraction peak indicate that the nanoparticle is well crystalline in structure. However, in the case of 0.27 M (1:1) precursor concentration, there were slight broader peaks that indicate smaller size ZnO nanoparticles were synthesized and which was consistent with the calculated crystalline size using Scherrer equation. The calculated crystalline size was 24.9 nm, 27.8 nm and 28.3 nm for 0.27 M, 0.36 M and 0.55 M of zinc acetate, respectively. It can be concluded that the synthesized ZnO NPs with 0.27 M of precursor concentration has the smallest average crystallite size and therefore the precursor concentration 0.27M (1:1) was considered for further studies.

XRD pattern of pure ZnO, CuO and ZnO/CuO composites are presented in Figure 6(b). As discussed above the XRD results of pure ZnO demonstrate the hexagonal wurtzite structure of ZnO. Similarly, XRD patterns of pure CuO is present in Figure 6(b). The peaks appeared at 2θ values of 32.55 º, 35.57 º, 38.77 º, 48.87 º, 53.50 º, 58.23 º, 61.59 º, 66.138 º, 68.02 º, 72.40 º and 75.10 º, and well matched with miller plane (1 1 0), (0 0 2), (1 1 1), (2 0 2), (0 2 0), (2 0 2), (1 1 3), (3 1 1), (1 1 3),(3 1 1) and (0 0 4) respectively which reveal the crystalline plane of CuO

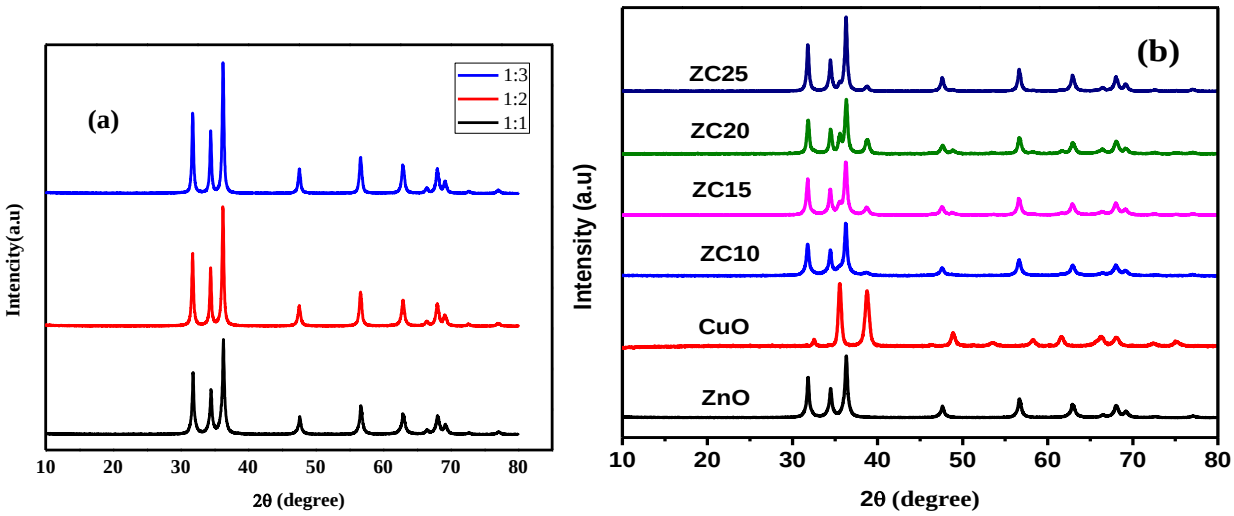

monoclinic phase (JCPDS CuO 048-1548) [103].

Figure 6. XRD result of the as synthesized ZnO, CuO, ZnO/CuO (10%),15%, 20% and 25%)

In ZnO/CuO nanocomposites other than the peaks of hexagonal crystalline phase of ZnO, the reflection peaks of CuO were observed at 2θ values of 32.54,35.57°, 38.7°, 48.84°, 53.48° and 58.16° which match to the (1 1 0), (0 0 2), (1 1 1), (2 0 2), (0 2 0), and (2 0 2), respectively which reveal the crystalline plane of CuO monoclinic phase (JCPDS CuO 048-1548) [103]. There is no additional peak in the nanocomposite, indicating the synthesized nanocomposite is purely composed of ZnO and CuO NPs without impurity [104].

The Samples ZC10, ZC15, ZC20 and ZC25 shows the XRD pattern of coupled ZnO/CuO composites with different wt% of copper nitrate. The addition of copper nitrate of 10 wt% (ZC10) show the reflection peaks of CuO with low intensity which is attributed to the low content of CuO in the sample. However, with an increase in the copper content (15% to 25%), CuO peaks have been observed with increased intensity. Furthermore, minor shifts were observed in the 2θ values of ZnO/CuO nanocomposite. The shift from 31.84◦ to 31.76◦, 34.49◦ to 34.41◦, and 36.32◦ to 36.23◦ were observed that indicate the typical peak of ZnO was changed. The trivial shifts indicate that the modification of ZnO with CuO can affect the structure of ZnO [88].

The Scherrer's equation (Eq.2) was applied to calculate the average crystallite size of the prepared samples [105]

$$D = \frac{K\lambda}{B\cos\Theta} \qquad (2)$$

where *K* is Scherrer's constant, which is 0.9, λ is the wavelength of the X-ray radiation which is 0.15406 nm, β is peak width at half maximum, and θ is Bragg's angle. Hence, the average crystallite for the all samples were calculated and reported in Table 3.

Table 3. Average crystalize size of as synthesized samples

S.No	Sample code	Average crystallite size (nm)
1	1:1	24.9

2	1:2	27.8
3	1:3	28.2
4	CuO	17
5	ZC10	22.9
6	ZC15	22.6
7	ZC20	22.6
8	ZC25	22.7

Mohammadi et al [87] synthesized ZnO without plant using microwave-assisted method and get particle size of 29 nm. The synthesized ZnO NPs in this work have particle size between 24 and 28 which is smaller than that of ZnO synthesized without plant extract. Likewise Ruan et al. [106] synthesis ZnO/CuO photocatalyst without plant and obtain particle size between 32 and 35. In the case of our study we found particle size of 23 nm for ZnO/CuO photocatalyst. This can be attributed to the presence of different functional groups including C–O, C=O, and O–H in *Musa acuminata* peel. These molecules stabilize particles of ZnO during their growth and formation of smaller particles of the ZnO. Similar results have been observed during fabrication of ZnO particles by using various plant extracts [107, 108].

4.3. SEM Analysis

SEM analysis was carried out to find the surface morphology of zinc oxide, copper oxide and ZnO/CuO nanocomposite using JCM-6000 scanning electron microscope at different magnification levels and results were shown in Figures 7 and 8.

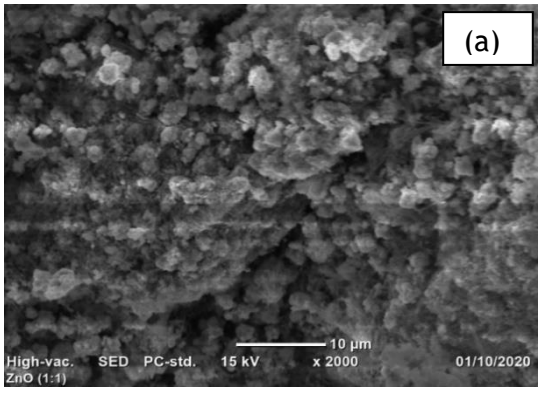

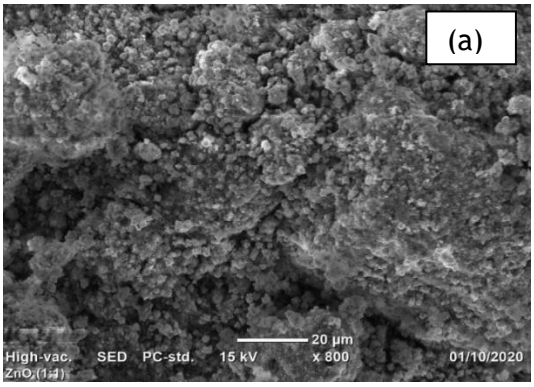

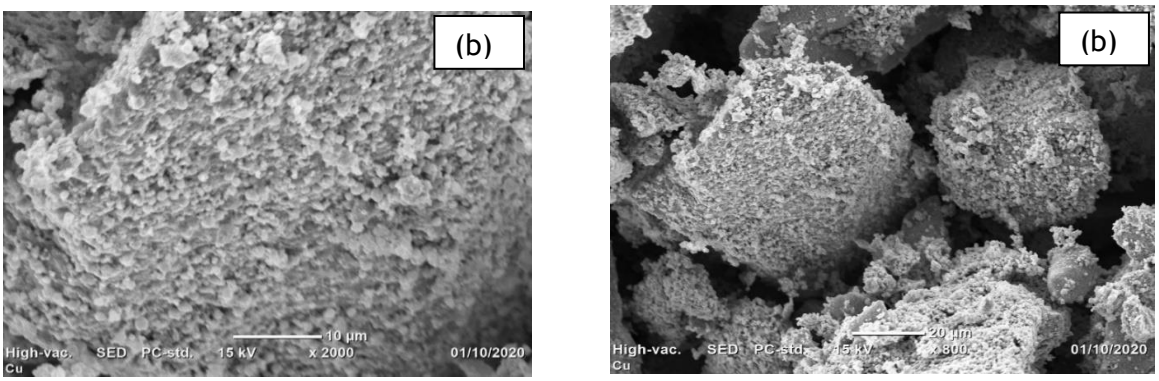

Figure. 7 SEM image of pure ZnO NPs (a) and CuO NPs (b).

The micrographs (Figures 7 a and b) showed that the network formation occurred at the zinc oxide and copper oxide nanoparticles with nearly spherical shape.

Figure 8 shows the SEM image of ZnO/CuO nanocomposite with different magnifications. As shown ZC20 nanocomposite has a cotton-like porous structure which is favorable for increasing the interaction between the photocatalyst surface and the organic pollutant that lead to enhancing the photodegradation efficiency [109].

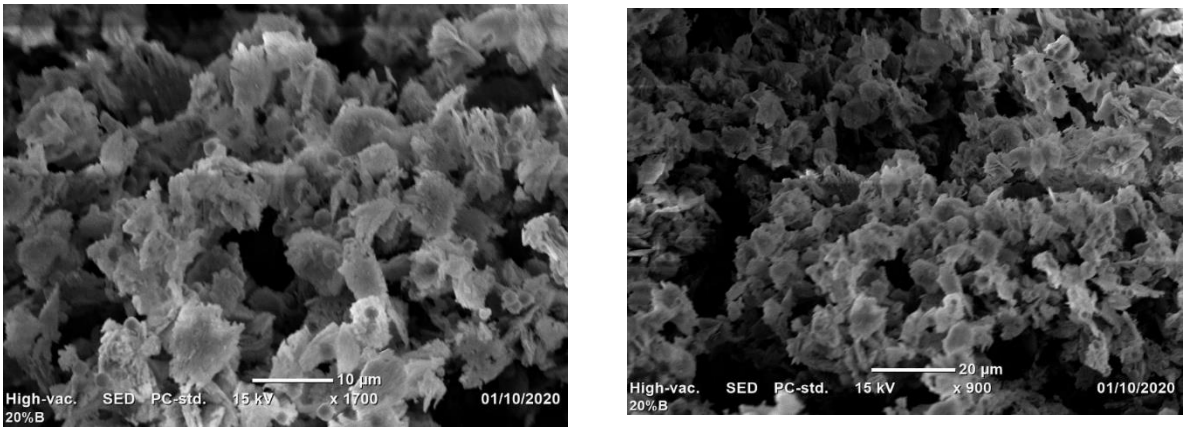

Figure 8. SEM image of ZnO/CuO nanocomposite with different magnifications.

4.4. FTIR analysis

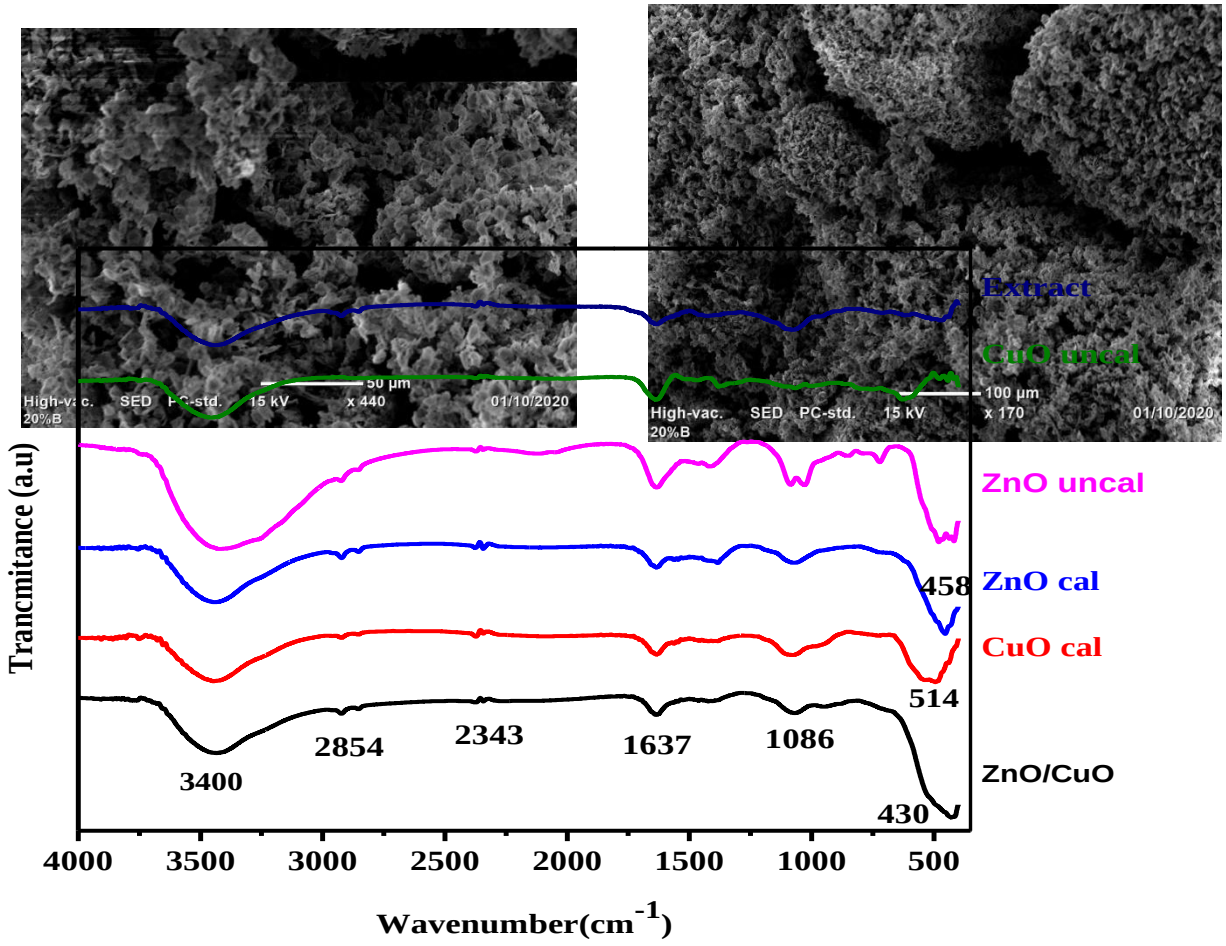

FT-IR spectra were also recorded to determine the functional groups of the samples in the range of 400–4000 cm^{-1}.The FT-IR spectra of the peel extract and prepared samples are shown in Figure 9.

Figure 9. FTIR spectra of BP extract, uncalcined ZnO, uncalcined CuO Calcined ZnO, calcined CuO and ZnO/CuO 20%.

The FT-IR spectra of the banana peel (BP) extract and all samples showed broad absorption band between 3400–3700 cm^{-1}, representing stretching vibration of O–H group [110],which confirm the presence of hydroxyl groups from the polyphenolic compounds of BP extract in the synthesis of NPs [97].

The spectra of ZnO NPS , CuO NPs, and ZC20% nanocomposite exhibited a band at wavenumbers of 2854 and 2922 cm^{-1}, which were ascribed to the stretching vibration of C-H bond in CH_2 and CH_3 groups respectively [111]. The weak band located at around 2280 cm^{-1} were attributed to $C-H$ stretching in aldehyde and the band near 2343 cm^{-1} could be the absorption of atmospheric CO_2 on the metallic cations [112]. In addition, the absorption peaks for carbonyl C=O stretching and O-H bending in alcohol were observed at 1637 and 1411 cm^{-1}, respectively [88]. The peaks around 1086 cm^{-1} and 1040 cm^{-1} were due to C-O stretching in secondary alcohol [113] and C-N stretching modes of aliphatic amines respectively [114]. Furthermore, slight bands at 730-630 cm^{-1},830 cm^{-1} and at 960 cm^{-1} may corresponds to C=C bending vibrations of alkenes [114].Those peaks disappear in the calcined samples as they burned out.

The absorption peaks around 458 cm^{-1} and 410 cm-1 in both calcined and un calcined ZnO samples are assigned to Zn-O bond similar to another report [115] that the vibration of Zn-O appeared in the range of 542-424 cm^{-1}. The wavenumbers of 544-486 cm^{-1} in both calcined and un calcined CuO samples are assigned to Cu-O bond according to reference [116] that the vibrations of the Cu-O are in the range of 600-490 cm^{-1}.

The peak in the range 543-430 cm^{-1} for the coupled metal oxide ZnO/CuO corresponds to the combined absorptions of Zn–O and Cu–O bonds. The shift of wavenumber at 458-400 cm^{-1} (Zn-O bond) were observed as the CuO is added to ZnO. The shift of wavenumber indicated that the addition of CuO may change the structure of ZnO NPs. What's important is that the FT-IR spectrum of ZnO/CuO sample displays a low intensity at 1411, 1040, 730,830 and 960 cm^{-1}, indicating the decrease of concentration of organic molecules of BP after calcination. However,

some organic functional groups have not been completely removed after calcination and still their vibration bands appeared in the calcined sample. This may be due to the short calcination time of NPs i.e. for 2 hrs.

4.5. UV-Vis spectroscopy analysis

The optical absorption properties of the as-prepared samples are characterized using UV–Vis diffuse reflectance spectra (DRS) and dipicted in Figure 10 (a-d). Figure 10 (a) show the absorption spectra of the green synthesized ZnO samples with different precursor concentration. From the spectra it was noticed that intensity of light absorption by ZnO NPs increases between 387 nm and 400 nm with increase in concentration of Zinc acetate. The increase in absorption intensity could be due to the increase in the crystalline size with precursor concentration which have close agreement with previous similar report [114].

The bandgap determination of ZnO NPs was carried out by Tauc plots as illustrated in Figure 9(b). Accordingly, the band gap energies were found to be 3.24, 3.25 and 3.24 ev, for 1:1,1:2 and 1:3 samples, respectively and have close agreement with previous study reports [117, 118]. The band gap of all the as synthesized ZnO samples are smaller than the band gap of the bulk ZnO (3.37 eV). The decrease in band gap of ZnO synthesized with plant extract is attributed to the quantum confinement effect [119].

Figure 10 (c) shows the absorption spectra of the green synthesized samples of ZnO, CuO, ZC10%, ZC1%, ZC20% and ZC 25%. As indicated on the graph all nanoparticles exhibit strong absorption peaks around 390 nm. However, the band edges of the peaks of the nanocomposites are extended into the visible region, indicating that the introduction of CuO creates additional states in the band gap of ZnO, resulting in the red shift of the band edge of the nanocomposites.

The absorption intensities of ZC composites were all obviously higher compared to pure ZnO. Further observation demonstrates that the absorbance in the visible light region and UV light region increases with Cu dosage, and all the benefits that come from the synergistic effect of CuO and ZnO. It is clearly observed that the appropriate CuO adding into ZnO leads to a red shift in the optical absorption edge, which could be due to the strong interfacial coupling between ZnO and CuO NPs [120]. This red-shift in absorption would be important for the photocatalytic degradation of MB dye.

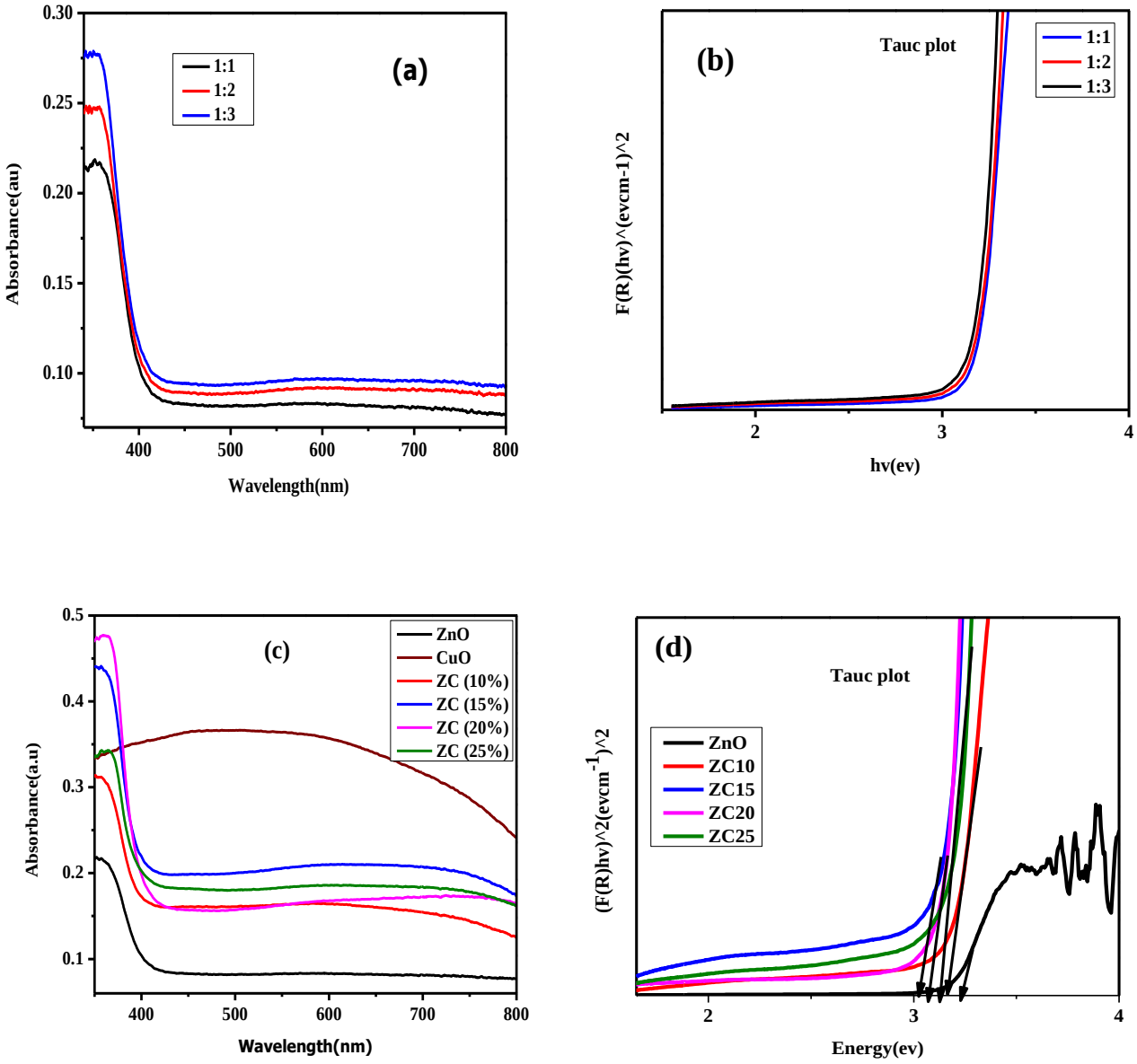

Figure 10. a) UV-Vis DRS spectra of ZnO NPs synthesized from different precursor concentrations; b) Tauc plot ($[F(R).hv$ vs $hv]^2$) of ZnO NPs synthesized from different precursor concentration's; c)UV-Vis DRS of ZnO, CuO, and ZC; and d) Tauc plot ($[F(R).hv$ vs $hv]^2$) of ZnO and ZC.

The band gap energies (Eg) of ZnO/CuO composites can be calculated based on the Kubelka-Munk theory.

$$[F(R)hv]^n = A(hv - Eg) \quad (3)$$

$$F(R) = \frac{1-R^2}{2R} \quad (4)$$

where R is the percentage of reflected light, h is the Planck constant, *v* is incident light frequency, n is the power index that is related to the characteristics transition in a semiconductor, and A is proportional constant depending on transition probability, respectively [73]. By plotting the $[F(R)hv]^n$ versus the photon energy (h*v*) and extrapolating the linear region of the curve to the energy axis, the optical band gaps can be estimated.

Figure 10 (d) illustrated the Tauc plot of ZnO, ZC10, ZC15, ZC20 and ZC25 samples and Eg value was found to be 3.24, 3.17, 3.14, 3.08 and 3.05, respectively which are in good agreement with the previous works [99, 121].The observed bandgap narrowing with the loading of CuO content was ascribed to the formation of interfacial contact among ZnO NPs and CuO NPs [120] and due to ZnO network defects as a result of incorporation of CuO [122]. The narrower band gap suggests easier excitation for an electron from the valence band to the conduction band in the oxide semiconductor. Hence, UV– Vis DRS results confirmed that ZnO/CuO nanocomposite can work as photocatalyst in the visible light area.

4.6. Photocatalytic activity

The photocatalytic activity of pure ZnO NPs, CuO NPs and ZnO/CuO nanocomposites were investigated for the decomposition of MB as a model pollutant under visible light irradiation. Figure 9 (a and b) illustrates the absorption spectra for the decomposition of MB dye solution under visible light by using photocatalyst ZnO and CuO respectively. Pure ZnO shows photocatalytic activity of 57 % which should be ascribed to the numerous oxygen vacancies on the ZnO surface, [123] while the lower photocatalytic activity (50%) of CuO could be as a result of rapid recombination of photogenerated electrons and holes.

All the ZnO/CuO composites have better photocatalytic performance (Figure 10) than pure ZnO and CuO NPs. The higher photocatalytic activity of ZnO/CuO nanocomposite could be associated with copper oxide, which acts as electron trap that inhibits e^{-}/h^{+} recombination. Furthermore, the synergistic effect of ZnO and CuO nanostructured semiconductor could enhance photocatalytic activity by forming heterojunction at the interface of the two semiconductors [124].

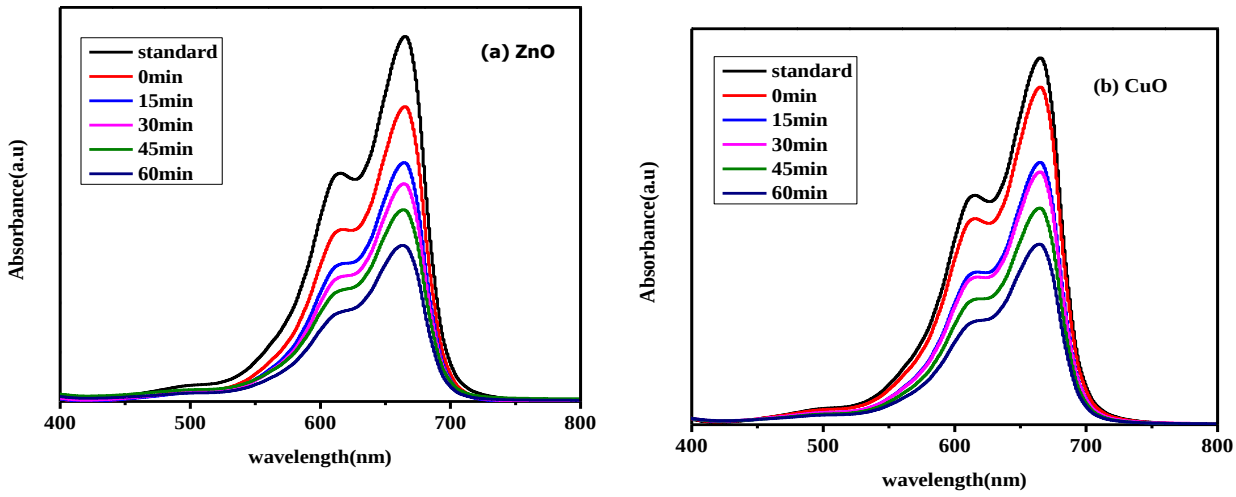

Figure 11. UV–visible spectra showing the reduction in the intensity of MB dye solution under visible light by using photocatalyst ZnO (a) and CuO (b).

4.6.1. Effect of CuO loading

Many reports have suggested that there is an optimum CuO loading in CuO/ZnO nanocomposites [125, 126]. Therefore, this study also attempted to investigate the optimum CuO loading in the ZC

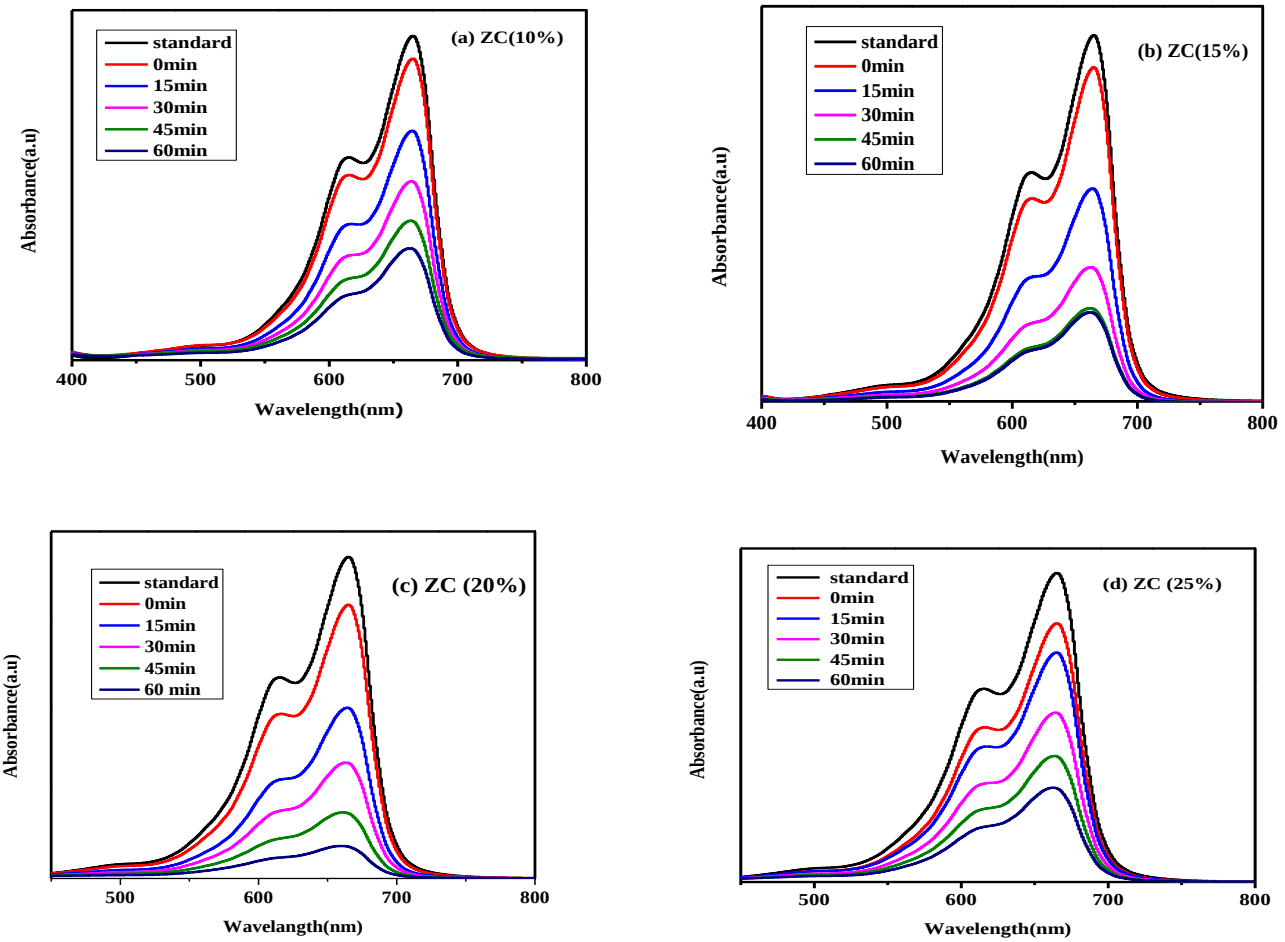

Figure 12. UV–visible spectra showing the reduction in the intensity of MB dye solution under visible light by using photocatalyst ZC10, ZC15, ZC20 and ZC25 (a-d).

photocatalyst. Figure 12 (a-d) shows the reduction of MB dye solution under visible light by using ZnO/CuO photocatalyst with different CuO loadings (from 10-25% of CuO into ZnO) and illustrate the degradation rate of MB is raise with CuO loading.

Furthermore, Figure 13 (a) also illustrate that the degradation efficiency is increased with CuO loading up to 20% CuO content and decreased for further increase to (25%) of CuO. The variation of the photocatalytic efficiency should be mainly connected with the change of CuO crystallite size as observed in XRD analysis. When CuO crystallites gradually grow up, the crystalline quality is improved, which is favorable for photogenerated electrons and holes to migrate to crystal surface

However, with the further grown-up of CuO crystallites, photocatalytic activity was declined. These could be related to two main reasons; firstly as CuO crystalline is grown, charge carriers need more time to migrate to crystal surface to participate redox reactions, which increases the possibility of the recombination of photogenerated electrons and holes inside the crystallites [127] ;secondly the over dose of CuO could blocked the active site of ZnO [128]. Sherly et al. [129] also reported similar results. It means that the ratio of CuO to ZnO in the CuO/ZnO nanocomposites is very important for the photocatalytic application.

Th plot of ln(C/C0) Vs irradiation time gives the rate constant for the synthesized samples as shown in Figure 13 (b and c). The rate constant for ZnO, CuO, ZC10, ZC15, ZC20 and ZC25 samples were found to be 0.007, 0.006, 0.015,0.022,0.035 and 0.016/min respectively. Among them, the ZC20 possess the highest degradation constant (0.035/min) which is about 5 times higher than ZnO (0.007/min).

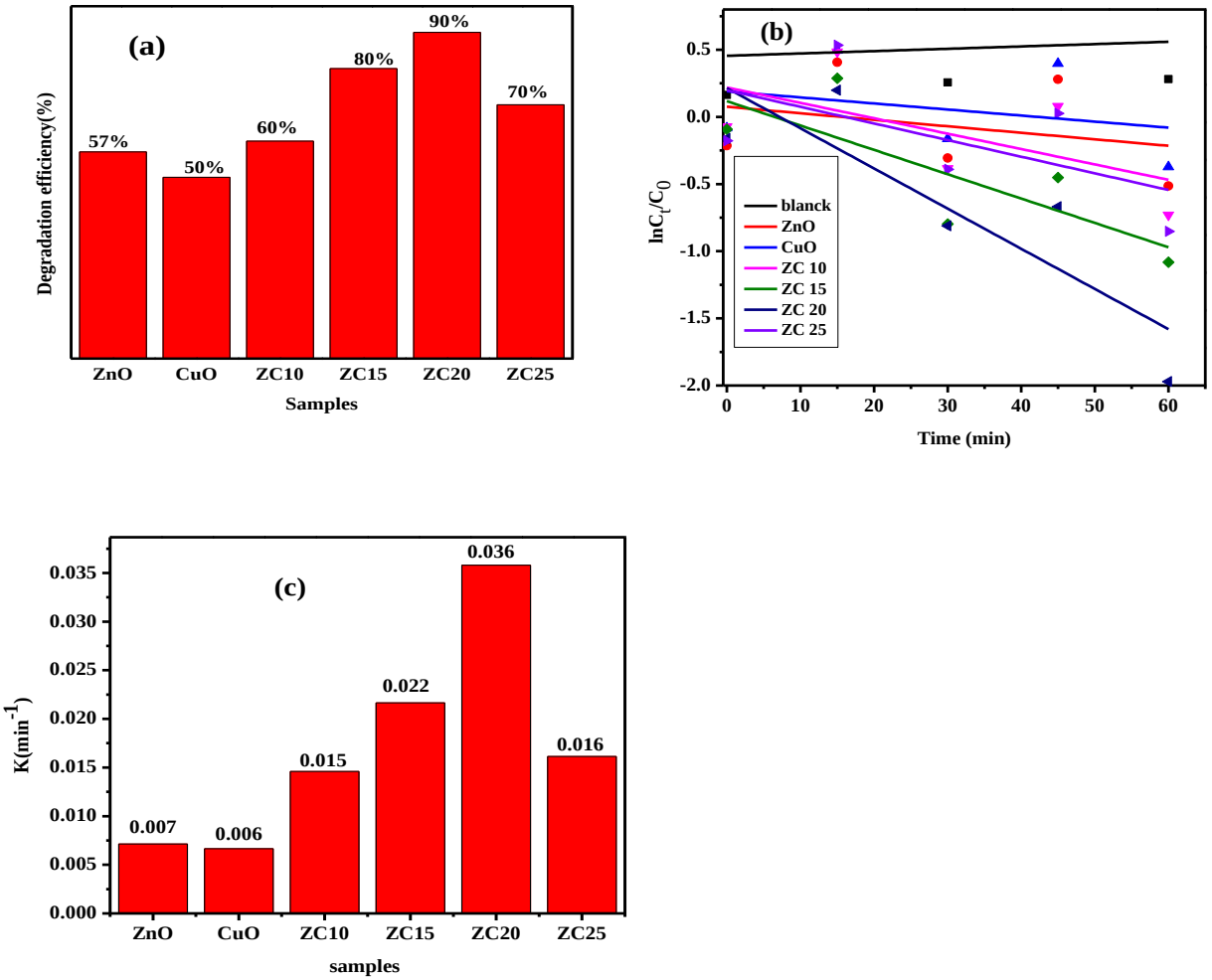

Figure 13. Bar graph revealing photocatalytic degradation efficiency of MB by different sample (a), photodegradation rate kinetics of MB (b) and bar graph revealing the variation in the rate constants for the degradation of MB dye under visible light by different samples.

4.6.2. Effect of solution pH

It is widely reported that due to varying interaction between catalyst and pollutant in different medium, dye solution pH plays a significant role in photodegradation reaction. In this study, 35mg ZC nano-composites with MB concentration of 10mg/L were exposed to visible light irradiation. The photocatalytic activity was tested at pH 4,7 and 10 using 1M NaOH and 1M HCl

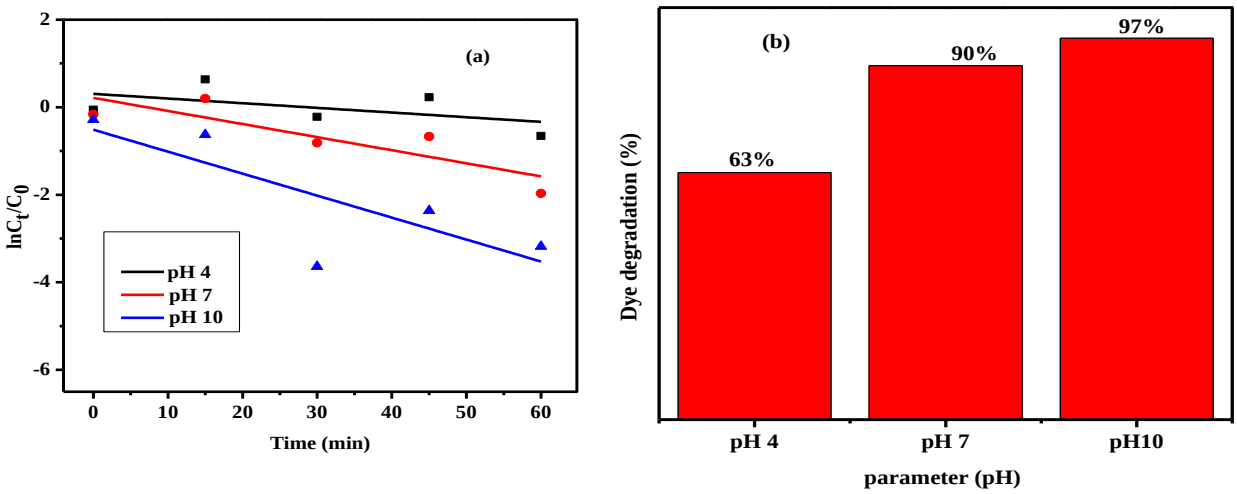

Figure 14. photodegradation rate kinetics of MB at different pH of solution(a) and corresponding degradation efficiency (b).

The results are plotted in Figure14 (a and b), which demonstrates that under acidic conditions, the degradation efficiency of the samples was limited. However, as the pH increases to neutral and alkaline values, the degradation ability of the samples gradually increases from 63% to 97% with K value of 0.0161,0.031 and 0.050/min. This is based on the variation in electrostatic forces existing between MB molecules and catalyst surface at different pH. The surface of the nanocomposite is negatively charged in an alkaline medium and positively charged in acidic medium. Because MB is a cationic dye, its structure becomes positively charged when it is dissolved in water. Unsurprisingly, the degradation rate of MB is therefore higher in alkaline media

due to an increase in opposite-charge interactions between the solution and the surface of the nano-composite [130].

4.6.3. Effect of the catalyst dosage

The influence of the photocatalyst dosage on the degradation of MB using ZC nanocomposites was studied by making the amount of photocatalyst 10 mg, 25mg, 35 mg and 50 mg under neutral conditions with an initial MB concentration of 10 mg/L. The results are displayed in Figure 15(a and b). As displayed on ln C/Co graph (a) and dye degradation bar graphs (b) increasing the photocatalyst dosage from 10 mg to 35 mg resulted in an increase in the reaction rate and degradation efficiency of MB.

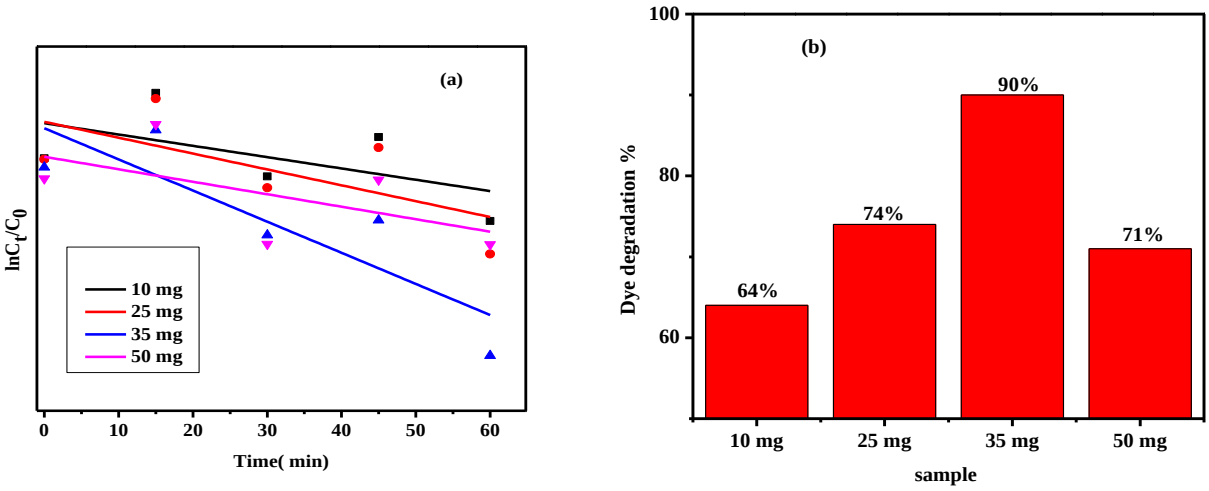

Figure 15. photodegradation rate kinetics of MB with various ZC catalyst dosage (a) and corresponding degradation efficiency (b).

However, at higher photocatalyst dosages (50 mg), the degradation efficiency tended to decrease. The reason generally advanced for this result is that increasing the amount of photocatalyst increases the available surface area or the number of active sites on the photocatalyst surface, which consequently increases the number of hydroxyl and superoxide radicals. However, as the amount of solid catalyst increases, the transparency of the solution decreases. The scattering of

light in the suspension prevents light from reaching some particles, and thus, some of the photocatalyst surface becomes unavailable for light absorption [131]. Therefore, above the optimum amount of catalyst, the degradation efficiency decreases due to the increased opacity of the suspension.

4.6.4. Effect of initial concentration of MB solution

The effect of initial MB concentration was investigated by using 5 mg/L,10 mg/L and 20 mg/L of MB concentration with 35 mg ZC photocatalyst under neutral condition. The results are shown in Figure 13 (a and b). The results in the Figure show that the degradation efficiency is very high at low concentrations of organic dyes and gradually decreases as the dye concentration increases.

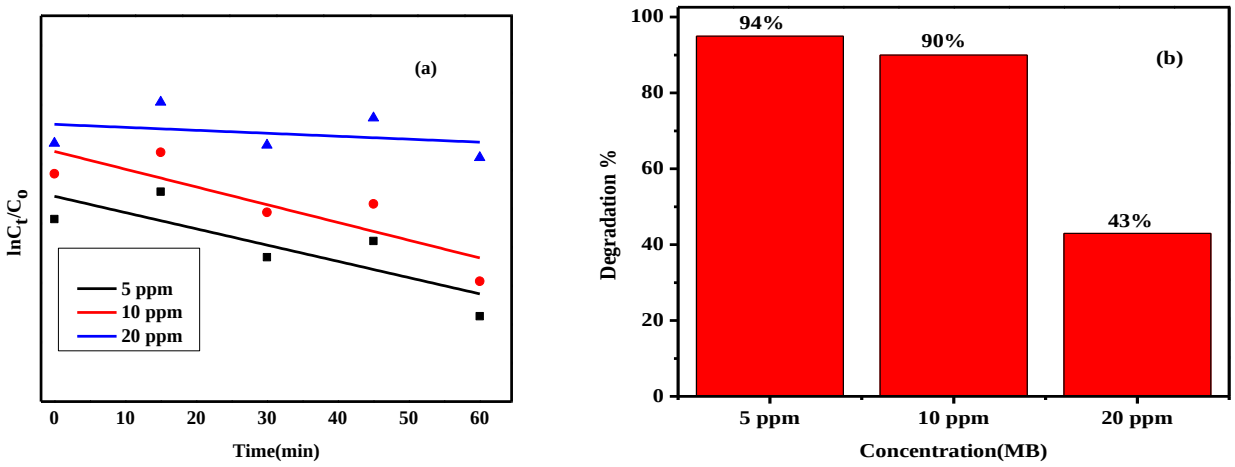

Figure 16. photodegradation rate kinetics of MB using ZC nanocomposites with various initial dye concentrations (a) and corresponding degradation efficiency (b).

Since the rate of degradation is proportional to the number of hydroxyl radicals and superoxide ions (*OH/O^-) formed at photocatalysts surface, increasing dye molecules could block more active sites and reduce the interaction of light with these sites for *OH generation. Another possible explanation for this result is the effect of light irradiation in the organic dyes. At a high dye concentration, a significant amount of light can be absorbed by the dye molecules rather than by

the photocatalysts, resulting in decreases in the formation of hydroxyl radicals (*OH) and superoxide ions ($*O^-$) and in the photocatalytic activity [132].

4.7. Reusability of the ZC nanocomposites

The lifespan of photocatalysts is an important parameter for practical applications. Therefore, the reusability of the photocatalysts was evaluated. In this experiment, ZC nanocomposites were recovered from the solution by centrifugation and washing with water several time. The recycled nanocomposite was used as photocatalysts for four repetitive experiments. The stability was evaluated by reusing the photocatalyst with the same quantity of fresh MB after each run. The results are summarized in Figure 17, which shows that after four cycles, MB photodegradation efficiencies of the samples. In addition, XRD was performed on the catalyst after four cycles and the results is depicted in Figure 17(b). The XRD results show that all diffraction peaks of the ZC nanocomposites remain the same before and after multiple catalytic reaction cycles suggesting an anti-photo-corrosion of ZC20 [133].

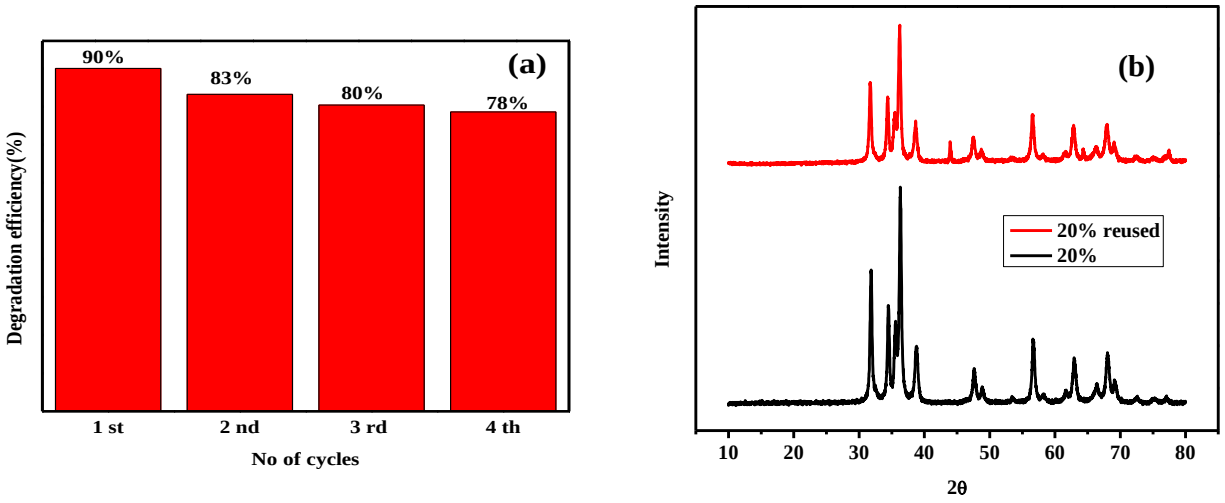

Figure 17 Degradation of MB in four cycles under visible irradiation (a) and XRD result of ZC photocatalyst after reused four times (b).

4.8. Mechanism of photodegradation

ZnO and CuO possess convenient band edge position with respect to charge carrier transfer, i.e. both the valence band (VB) and conduction band (CB) of CuO lies above than ZnO, which is thermodynamically favorable for transfer of electrons and holes between them [134].

Upon absorbing Visible light, electron starts exciting from VB to CB with generation of holes in VB in both the semiconductor. As VB and CB of ZnO lies lower than that of CuO, electrons start moving from uphill CB of CuO to lower level CB of ZnO while photoinduced holes start moving from low level VB of ZnO to higher level CB of CuO in opposite direction at the interface of ZnO/CuO hetero-junction. As a result, more electrons are piled in CB of ZnO that are used for the reduction of MB.

Such type of electron transfer inhibits recombination of charge carriers i.e. electron-hole pair which results in enhancement of photodegradation efficiency. The electrons in CB of ZnO were trapped by molecular oxygen present on the surface of ZnO to form superoxide radicals ($O_2^{\cdot -}$). While photoinduced holes in VB were captured by hydroxide ion with generation of active species i.e. hydroxyl radicals. These free radical react with MB leading to complete mineralization of MB in CO_2 and H_2O [135].

As we calculated using Tauc plot the band gap (Eg) of ZnO and CuO is 3.14 eV and 1.7 eV respectively. whereas the electron affinity of ZnO and CuO was reported to be 4.35 eV and 4.07 eV, respectively [136, 137]. Based on these results, we propose a possible photocatalytic mechanism of the degradation of MB under visible-light irradiation as in Figure 18 and eq (5-11).

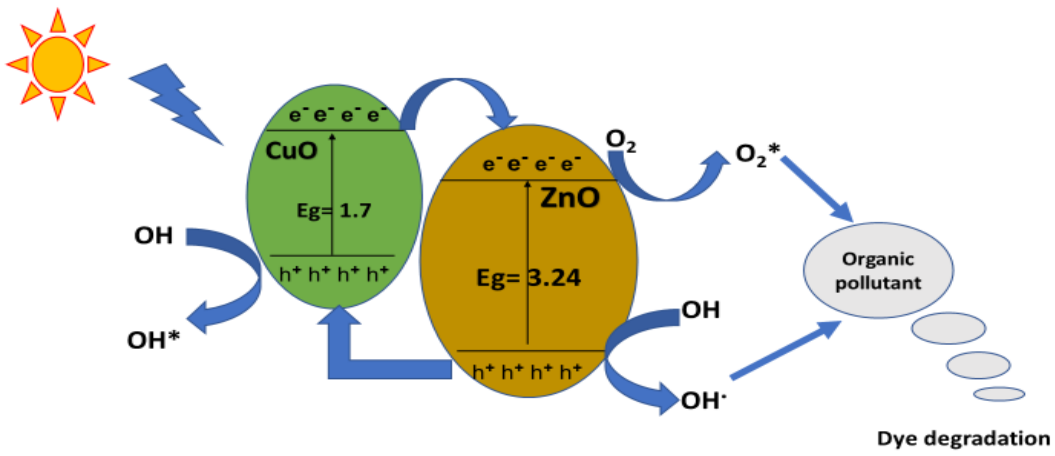

Figure 18. schematic diagram for photodegradation mechanism by ZC nanocomposite under visibile light.

$$ZnO(e^- + h^+)/CuO(e^- + h^+) \rightarrow ZnO(e^- + e^-) + /CuO(h^+ + h^+) \quad (5)$$

$$H_2O + h^+_{VB} \rightarrow OH^{-\cdot} + H^+ \quad (6)$$

$$O_2 + e^-_{CB} \rightarrow O_2^{-\cdot} \quad (7)$$

$$O_2^{-\cdot} + H^+ \rightarrow HO_2^- \quad (8)$$

$$HO_2^- + H^+ \rightarrow H_2O_2 \quad (9)$$

$$H_2O_2 + hv \rightarrow 2OH^{-\cdot} \quad (10)$$

MB when contact with $OH^{-\cdot}$ or $O_2^{-\cdot}$ → intermediates →harmless products +CO_2+H_2O (11)

5. Conclusion and recommendation

5.1. Conclusion

In this work, ZnO NPs, CuO NPs and CuO/ZnO nanocomposites were synthesized by a green sol gel method using *Musa acuminate* peel extract as capping agent. The structural studies revealed that synthesized ZnO/CuO nano-composites were found with purely hexagonal wurtzite ZnO and monoclinic CuO phase. Optical studies have showed the shift in absorption wavelength towards higher wavelength that confirms formation of ZnO/CuO hetero-junction and assured the bandgap narrowing with enhancement in the visible light absorption.

Compared with pure ZnO NPs and CuO NPs, the photocatalytic performance of the CuO/ZnO nanocomposites is largely improved, which is attributed to the band coupling between ZnO and CuO and the improvement of utilization efficiency of solar energy. It is found that pH of the dye solution, initial concentration of dye solution, catalyst loading and the CuO contents in the nanocomposite have a great influence on the photocatalytic performance. The optimum working conditions are at pH 10 of the dye solution, 5 mg/l of dye concentration with 30 mg of catalyst that give 97% degradation of MB dye in 60 min. The optimum concentration of CuO, (20 wt%) exhibits enhanced photocatalytic activity which is five times higher than pure ZnO.

The formation of ZnO/CuO hetero-junction improved the separation of photogenerated electrons and holes which results in enhanced photocatalytic activity. Thus, ZnO/CuO are considered a promising photocatalytic material to degrade organic pollutant in visible light.

5.2. Recommendations

For the future study, there are a few recommendations on the characterization of ZnO/CuO nanocomposites that will give full information. The elemental distribution and chemical composition of the synthesized samples should be characterized by energy depressive X-ray (EDX) and X-ray photoelectron spectroscopy (XPS). In order to investigate the particle size, more detail morphology and surface area of nanocomposite the samples should be characterized by TEM and BET instruments respectively. Furthermore, In order to identify which reactive species are mostly involved in the photodegradation of the MB, scavengers should be used during photoreaction.

Research Fund Acknowledgment

This research project is funded by Adama Science and Technology University under the grant number ASTU/SM-R/011/19, Adama, Ethiopia.

References

1. Chauhan, P.S., et al., *Facile synthesis of ZnO/GO nanoflowers over Si substrate for improved photocatalytic decolorization of MB dye and industrial wastewater under solar irradiation.* Materials Science in Semiconductor Processing, 2019. **89**: p. 6-17.
2. Nassar, M.Y., et al., *A controlled, template-free, and hydrothermal synthesis route to sphere-like α-Fe 2 O 3 nanostructures for textile dye removal.* Rsc Advances, 2016. **6**(24): p. 20001-20013.
3. Jokar, M., et al., *Preparation and characterization of novel bio ion exchanger from medicinal herb waste (chicory) for the removal of Pb2+ and Cd2+ from aqueous solutions.* Journal of Water Process Engineering, 2019. **28**: p. 88-99.
4. Pype, M.L., et al., *Reverse osmosis integrity monitoring in water reuse: The challenge to verify virus removal - A review.* Water Res, 2016. **98**: p. 384-95.
5. Dickhout, J.M., et al., *Produced water treatment by membranes: A review from a colloidal perspective.* J Colloid Interface Sci, 2017. **487**: p. 523-534.
6. Subramani, A. and J.G. Jacangelo, *Emerging desalination technologies for water treatment: a critical review.* Water Res, 2015. **75**: p. 164-87.
7. Miranda, A.C., et al., *Surface water disinfection by chlorination and advanced oxidation processes: Inactivation of an antibiotic resistant E. coli strain and cytotoxicity evaluation.* Sci Total Environ, 2016. **554-555**: p. 1-6.
8. Remucal, C. and D. Manley, *Emerging investigators series: the efficacy of chlorine photolysis as an advanced oxidation process for drinking water treatment.* Environmental Science: Water Research & Technology, 2016. **2**(4): p. 565-579.
9. Khaki, M.R.D., et al., *Application of doped photocatalysts for organic pollutant degradation - A review.* J Environ Manage, 2017. **198**(Pt 2): p. 78-94.
10. Khin, M.M., et al., *A review on nanomaterials for environmental remediation.* Energy & Environmental Science, 2012. **5**(8): p. 8075.
11. Hou, G., et al., *Controllable synthesis of CuS decorated TiO 2 nanofibers for enhanced photocatalysis.* CrystEngComm, 2015. **17**(29): p. 5496-5501.
12. Huang, Y.-C., S.-Y. Chang, and J.-M. Jehng, *Photocatalytic H2 generation efficiencies of TiO2 nanotube-based heterostructures grafted with ZnO nanorods, Ag nanoparticles, or Pd nanodendrites.* The Journal of Physical Chemistry C, 2017. **121**(35): p. 19063-19068.

13. Kanade, K., et al., *Self-assembled aligned Cu doped ZnO nanoparticles for photocatalytic hydrogen production under visible light irradiation.* Materials Chemistry and Physics, 2007. **102**(1): p. 98-104.
14. Phiwdang, K., et al., *Synthesis of CuO nanoparticles by precipitation method using different precursors.* Energy Procedia, 2013. **34**: p. 740-745.
15. Lu, P., et al., *Abnormal room temperature ferromagnetism in CuO/ZnO nanocomposites via hydrothermal method.* Applied Surface Science, 2017. **399**: p. 396-402.
16. Das, S. and V.C. Srivastava, *Synthesis and characterization of ZnO/CuO nanocomposite by electrochemical method.* materials science in semiconductor processing, 2017. **57**: p. 173-177.
17. Kaviyarasu, K., et al., *Synthesis and characterization studies of MgO: CuO nanocrystals by wet-chemical method.* Spectrochimica Acta Part A: Molecular and Biomolecular Spectroscopy, 2015. **142**: p. 405-409.
18. Gajendiran, J. and V. Rajendran, *Synthesis and characterization of coupled semiconductor metal oxide (ZnO/CuO) nanocomposite.* Materials Letters, 2014. **116**: p. 311-313.
19. Seabra, A.B. and N. Duran, *Nanotoxicology of metal oxide nanoparticles.* Metals, 2015. **5**(2): p. 934-975.
20. Jalali, S., et al., *One step integration of plasmonic Ag2CrO4/Ag/AgCl into HKUST-1-MOF as novel visible-light driven photocatalyst for highly efficient degradation of mixture dyes pollutants: Its photocatalytic mechanism and modeling.* Polyhedron, 2019. **166**: p. 217-225.
21. Zou, L., et al., *Fabrication and dye removal performance of magnetic CuFe2O4@CeO2 nanofibers.* Applied Surface Science, 2015. **332**: p. 674-681.
22. Kumar, P.S., et al., *CuO/ZnO nanorods: an affordable efficient pn heterojunction and morphology dependent photocatalytic activity against organic contaminants.* Journal of Alloys and Compounds, 2017. **701**: p. 562-573.
23. Kamel, N.A., S.L. Abd El-messieh, and N.M. Saleh, *Chitosan/banana peel powder nanocomposites for wound dressing application: Preparation and characterization.* Materials Science and Engineering: C, 2017. **72**: p. 543-550.

24. Owa, F., *Water pollution: sources, effects, control and management.* International Letters of Natural Sciences, 2014. **3**.
25. Chong, M.N., et al., *Recent developments in photocatalytic water treatment technology: a review.* Water Res, 2010. **44**(10): p. 2997-3027.
26. Konstantinou, I.K. and T.A. Albanis, *TiO2-assisted photocatalytic degradation of azo dyes in aqueous solution: kinetic and mechanistic investigations.* Applied Catalysis B: Environmental, 2004. **49**(1): p. 1-14.
27. Gupta, V.K., et al., *Chemical treatment technologies for waste-water recycling—an overview.* RSC Advances, 2012. **2**(16): p. 6380.
28. Rajeshwar, K., et al., *Heterogeneous photocatalytic treatment of organic dyes in air and aqueous media.* Journal of Photochemistry and Photobiology C: Photochemistry Reviews, 2008. **9**(4): p. 171-192.
29. Esplugas, S., et al., *Ozonation and advanced oxidation technologies to remove endocrine disrupting chemicals (EDCs) and pharmaceuticals and personal care products (PPCPs) in water effluents.* J Hazard Mater, 2007. **149**(3): p. 631-42.
30. Cheng, M., et al., *Hydroxyl radicals based advanced oxidation processes (AOPs) for remediation of soils contaminated with organic compounds: a review.* Chemical Engineering Journal, 2016. **284**: p. 582-598.
31. Byrne, C., G. Subramanian, and S.C. Pillai, *Recent advances in photocatalysis for environmental applications.* Journal of Environmental Chemical Engineering, 2018. **6**(3): p. 3531-3555.
32. Moniz, S.J.A., et al., *Visible-light driven heterojunction photocatalysts for water splitting – a critical review.* Energy & Environmental Science, 2015. **8**(3): p. 731-759.
33. Ponraj, C., V. G, and J. Daniel, *A review on the visible light active BiFeO 3 nanostructures as suitable photocatalyst in the degradation of different textile dyes.* Environmental Nanotechnology, Monitoring & Management, 2017. **7**: p. 110-120.
34. Khan, M.M., S.F. Adil, and A. Al-Mayouf, *Metal oxides as photocatalysts.* Journal of Saudi Chemical Society, 2015. **19**(5): p. 462-464.
35. Saravanan, R., et al., *PHOTOCATALYTIC DEGRADATION OF ORGANIC DYE USING NANO ZnO.* International Journal of Nanoscience, 2012. **10**(01n02): p. 253-257.

36. Gnanasekaran, L., R. Hemamalini, and K. Ravichandran, *Synthesis and characterization of TiO2 quantum dots for photocatalytic application.* Journal of Saudi Chemical Society, 2015. **19**(5): p. 589-594.
37. Farahmand, T., S. Hashemian, and A. Shibani, *ZIF@ZnTiO3 Nanocomposite as a Reusable Organocatalyst for the Synthesis of 3, 4-dihydropyrano[c]chromene Derivatives.* Current Organocatalysis, 2019. **6**(3): p. 248-256.
38. Liu, D., Z. Zhang, and J. Wu, *Elemental mercury removal by MnO2 nanoparticle-decorated carbon nitride nanosheet.* Energy & Fuels, 2019. **33**(4): p. 3089-3097.
39. Jang, E.S., et al., *Fine Tuning of the Face Orientation of ZnO Crystals to Optimize Their Photocatalytic Activity.* Advanced Materials, 2006. **18**(24): p. 3309-3312.
40. Salama, A., et al., *Photocatalytic degradation of organic dyes using composite nanofibers under UV irradiation.* Applied Nanoscience, 2018. **8**(1-2): p. 155-161.
41. Xin, Y., Q. Chen, and G. Zhang, *Construction of ternary heterojunction CuS-CdS/TiO2 nanobelts for photocatalytic degradation of gaseous toluene.* Journal of Alloys and Compounds, 2018. **751**: p. 231-240.
42. Kazeminezhad, I. and A. Sadollahkhani, *Influence of pH on the photocatalytic activity of ZnO nanoparticles.* Journal of Materials Science: Materials in Electronics, 2016. **27**(5): p. 4206-4215.
43. Reza, K.M., A.S.W. Kurny, and F. Gulshan, *Parameters affecting the photocatalytic degradation of dyes using TiO2: a review.* Applied Water Science, 2015. **7**(4): p. 1569-1578.
44. Kaur, J. and S. Singhal, *Heterogeneous photocatalytic degradation of rose bengal: effect of operational parameters.* Physica B: Condensed Matter, 2014. **450**: p. 49-53.
45. Farzana, M.H. and S. Meenakshi, *Visible light-driven photoactivity of zinc oxide impregnated chitosan beads for the detoxification of textile dyes.* Applied Catalysis A: General, 2015. **503**: p. 124-134.
46. Roy, N. and S. Chakraborty, *ZnO as photocatalyst: An approach to waste water treatment.* Materials Today: Proceedings, 2020.
47. Nor, M.N.M. and M. Shamsuddin, *Biosynthesis of zinc oxide nanoparticles using Ficus Auriculata (elephant ear fig) leaf extract and their photocatalytic activity.* eProceedings Chemistry, 2016. **1**(2).

48. Dhandapani, P., et al., *Ureolytic bacteria mediated synthesis of hairy ZnO nanostructure as photocatalyst for decolorization of dyes.* Materials Chemistry and Physics, 2020. **243**: p. 122619.
49. Wang, J., et al., *Cost-effective large-scale synthesis of oxygen-defective ZnO photocatalyst with superior activities under UV and visible light.* Ceramics International, 2017. **43**(2): p. 1870-1879.
50. Djurišić, A.B., Y.H. Leung, and A.M. Ching Ng, *Strategies for improving the efficiency of semiconductor metal oxide photocatalysis.* Materials Horizons, 2014. **1**(4): p. 400.
51. Nikokavoura, A. and C. Trapalis, *Alternative photocatalysts to TiO2 for the photocatalytic reduction of CO2.* Applied Surface Science, 2017. **391**: p. 149-174.
52. Zhu, D., et al., *High-performance self-powered/active humidity sensing of Fe-doped ZnO nanoarray nanogenerator.* Sensors and Actuators B: Chemical, 2015. **213**: p. 382-389.
53. Yayapao, O., et al., *Ultrasonic-assisted synthesis of Nd-doped ZnO for photocatalysis.* Materials Letters, 2013. **90**: p. 83-86.
54. Yun, S., et al., *Improvement of ZnO nanorod-based dye-sensitized solar cell efficiency by Al-doping.* Journal of Physics and Chemistry of Solids, 2010. **71**(12): p. 1724-1731.
55. Li, J. and N. Wu, *Semiconductor-based photocatalysts and photoelectrochemical cells for solar fuel generation: a review.* Catalysis Science & Technology, 2015. **5**(3): p. 1360-1384.
56. Yu, W., J. Zhang, and T. Peng, *New insight into the enhanced photocatalytic activity of N-, C- and S-doped ZnO photocatalysts.* Applied Catalysis B: Environmental, 2016. **181**: p. 220-227.
57. Sharma, S., S.K. Mehta, and S.K. Kansal, *N doped ZnO/C-dots nanoflowers as visible light driven photocatalyst for the degradation of malachite green dye in aqueous phase.* Journal of Alloys and Compounds, 2017. **699**: p. 323-333.
58. Sudrajat, H. and S. Babel, *A novel visible light active N-doped ZnO for photocatalytic degradation of dyes.* Journal of Water Process Engineering, 2017. **16**: p. 309-318.
59. Jeong, B., et al., *ZnO shell on mesoporous silica by atomic layer deposition: removal of organic dye in water by an adsorbent and its photocatalytic regeneration.* Applied surface science, 2014. **307**: p. 468-474.

60. Akhundi, A. and A. Habibi-Yangjeh, *Ternary g-C3N4/ZnO/AgCl nanocomposites: synergistic collaboration on visible-light-driven activity in photodegradation of an organic pollutant.* Applied Surface Science, 2015. **358**: p. 261-269.
61. Qin, R., et al., *Fabrication and enhanced photocatalytic property of TiO2-ZnO composite photocatalysts.* Materials Letters, 2019. **240**: p. 84-87.
62. Cho, S., et al., *Three-dimensional type II ZnO/ZnSe heterostructures and their visible light photocatalytic activities.* Langmuir, 2011. **27**(16): p. 10243-10250.
63. Shi, S., J. Xu, and L. Li, *Preparation and photocatalytic activity of ZnO nanorods and ZnO/Cu 2O nanocomposites.* Main Group Chemistry, 2017. **16**(1): p. 47-55.
64. Liu, H., et al., *One-step hydrothermal synthesis of In2O3–ZnO heterostructural composites and their enhanced visible-light photocatalytic activity.* Materials Letters, 2014. **131**: p. 104-107.
65. Lamba, R., et al., *Visible-light-driven photocatalytic properties of self assembled cauliflower-like AgCl/ZnO hierarchical nanostructures.* Journal of Molecular Catalysis A: Chemical, 2015. **408**: p. 189-201.
66. Harish, S., et al., *Functional properties and enhanced visible light photocatalytic performance of V3O4 nanostructures decorated ZnO nanorods.* Applied Surface Science, 2017. **418**: p. 171-178.
67. Saravanan, R., et al., *Visible light degradation of textile effluent using novel catalyst ZnO/γ-Mn2O3.* Journal of the Taiwan Institute of Chemical Engineers, 2014. **45**(4): p. 1910-1917.
68. Wang, C., et al., *Electrospinning direct synthesis of magnetic ZnFe2O4/ZnO multi-porous nanotubes with enhanced photocatalytic activity.* Applied Surface Science, 2017. **396**: p. 780-790.
69. Peng, F., et al., *Construction of ZnO nanosheet arrays within BiVO4 particles on a conductive magnetically driven cilia film with enhanced visible photocatalytic activity.* Journal of Alloys and Compounds, 2017. **690**: p. 953-960.
70. Devi, H.S. and T.D. Singh, *Synthesis of copper oxide nanoparticles by a novel method and its application in the degradation of methyl orange.* Advance in Electronic and Electric engineering, 2014. **4**(1): p. 83-88.

71. Katal, R., et al., *Nanocrystal-engineered thin CuO film photocatalyst for visible-light-driven photocatalytic degradation of organic pollutant in aqueous solution.* Catalysis Today, 2020. **340**: p. 236-244.
72. Kumari, V., et al., *Synthesis and characterization of heterogeneous ZnO/CuO hierarchical nanostructures for photocatalytic degradation of organic pollutant.* Advanced Powder Technology, 2020.
73. Zhu, L., et al., *Synthesis of the 0D/3D CuO/ZnO heterojunction with enhanced photocatalytic activity.* The Journal of Physical Chemistry C, 2018. **122**(17): p. 9531-9539.
74. Pirhashemi, M., A. Habibi-Yangjeh, and S. Rahim Pouran, *Review on the criteria anticipated for the fabrication of highly efficient ZnO-based visible-light-driven photocatalysts.* Journal of Industrial and Engineering Chemistry, 2018. **62**: p. 1-25.
75. Yu, J., et al., *Photogenerated electron reservoir in hetero-p–n CuO–ZnO nanocomposite device for visible-light-driven photocatalytic reduction of aqueous Cr (VI).* Journal of Materials Chemistry A, 2015. **3**(3): p. 1199-1207.
76. Li, B. and Y. Wang, *Facile synthesis and photocatalytic activity of ZnO–CuO nanocomposite.* Superlattices and Microstructures, 2010. **47**(5): p. 615-623.
77. Sathishkumar, P., et al., *Synthesis of CuO-ZnO nanophotocatalyst for visible light assisted degradation of a textile dye in aqueous solution.* Chemical Engineering Journal, 2011. **171**(1): p. 136-140.
78. Minh, T.T., et al., *Synthesis of Porous Octahedral ZnO/CuO Composites from Zn/Cu-Based MOF-199 and Their Applications in Visible-Light-Driven Photocatalytic Degradation of Dyes.* Journal of Nanomaterials, 2019. **2019**: p. 1-16.
79. Muzakki, A., H. Shabrany, and R. Saleh. *Synthesis of ZnO/CuO and TiO2/CuO nanocomposites for light and ultrasound assisted degradation of a textile dye in aqueous solution*. in *AIP Conference Proceedings*. 2016. AIP Publishing.
80. Mansournia, M. and L. Ghaderi, *CuO@ZnO core-shell nanocomposites: Novel hydrothermal synthesis and enhancement in photocatalytic property.* Journal of Alloys and Compounds, 2017. **691**: p. 171-177.

81. Hassanpour, M., et al., *Nano-sized CuO/ZnO hollow spheres: synthesis, characterization and photocatalytic performance.* Journal of Materials Science: Materials in Electronics, 2017. **28**(19): p. 14678-14684.
82. Saravanan, R., et al., *Enhanced photocatalytic activity of ZnO/CuO nanocomposite for the degradation of textile dye on visible light illumination.* Materials Science and Engineering: C, 2013. **33**(1): p. 91-98.
83. Dobrucka, R. and J. Długaszewska, *Biosynthesis and antibacterial activity of ZnO nanoparticles using Trifolium pratense flower extract.* Saudi Journal of Biological Sciences, 2016. **23**(4): p. 517-523.
84. Dhanemozhi, A.C., V. Rajeswari, and S. Sathyajothi, *Green synthesis of zinc oxide nanoparticle using green tea leaf extract for supercapacitor application.* Materials Today: Proceedings, 2017. **4**(2): p. 660-667.
85. Madhukara Naik, M., et al., *Green synthesis of zinc ferrite nanoparticles in Limonia acidissima juice: Characterization and their application as photocatalytic and antibacterial activities.* Microchemical Journal, 2019. **146**: p. 1227-1235.
86. Nava, O., et al., *Fruit peel extract mediated green synthesis of zinc oxide nanoparticles.* Journal of Molecular Structure, 2017. **1147**: p. 1-6.
87. Mohammadi-Aloucheh, R., et al., *Green synthesis of ZnO and ZnO/CuO nanocomposites in Mentha longifolia leaf extract: characterization and their application as anti-bacterial agents.* Journal of Materials Science: Materials in Electronics, 2018. **29**(16): p. 13596-13605.
88. Yulizar, Y., et al., *ZnO/CuO nanocomposite prepared in one-pot green synthesis using seed bark extract of Theobroma cacao.* Nano-Structures & Nano-Objects, 2018. **16**: p. 300-305.
89. Saputra, I. and Y. Yulizar. *Biosynthesis and characterization of ZnO nanoparticles using the aqueous leaf extract of Imperata cylindrica L*. in *IOP Conference Series: Materials Science and Engineering*. 2017. IOP Publishing.
90. Matinise, N., et al., *ZnO nanoparticles via Moringa oleifera green synthesis: physical properties & mechanism of formation.* Applied Surface Science, 2017. **406**: p. 339-347.

91. Elumalai, K., et al., *Bio-approach: plant mediated synthesis of ZnO nanoparticles and their catalytic reduction of methylene blue and antimicrobial activity.* Advanced Powder Technology, 2015. **26**(6): p. 1639-1651.
92. Sone, B., et al., *Biosynthesized CuO nano-platelets: physical properties & enhanced thermal conductivity nanofluidics.* Arabian Journal of Chemistry, 2017.
93. Sharma, J.K., et al., *Green synthesis of CuO nanoparticles with leaf extract of Calotropis gigantea and its dye-sensitized solar cells applications.* Journal of Alloys and Compounds, 2015. **632**: p. 321-325.
94. Nasrollahzadeh, M., et al., *Green synthesis of Pd/CuO nanoparticles by Theobroma cacao L. seeds extract and their catalytic performance for the reduction of 4-nitrophenol and phosphine-free Heck coupling reaction under aerobic conditions.* Journal of colloid and interface science, 2015. **448**: p. 106-113.
95. Bordbar, M., N. Negahdar, and M. Nasrollahzadeh, *Melissa Officinalis L. leaf extract assisted green synthesis of CuO/ZnO nanocomposite for the reduction of 4-nitrophenol and Rhodamine B.* Separation and Purification Technology, 2018. **191**: p. 295-300.
96. Ibrahim, H.M., *Green synthesis and characterization of silver nanoparticles using banana peel extract and their antimicrobial activity against representative microorganisms.* Journal of Radiation Research and Applied Sciences, 2015. **8**(3): p. 265-275.
97. Vijayakumar, S., et al., *Therapeutic effects of gold nanoparticles synthesized using Musa paradisiaca peel extract against multiple antibiotic resistant Enterococcus faecalis biofilms and human lung cancer cells (A549).* Microbial pathogenesis, 2017. **102**: p. 173-183.
98. Ertaş, A., et al., *Evaluation of Antioxidant, Cholinesterase Inhibitory and Antimicrobial Properties of Mentha longifolia subsp. noeana and Its Secondary Metabolites.* Records of Natural Products, 2015. **9**(1).
99. Cahino, A.M., et al., *Characterization and evaluation of ZnO/CuO catalyst in the degradation of methylene blue using solar radiation.* Ceramics International, 2019. **45**(11): p. 13628-13636.

100. Bayrami, A., et al., *Bio-extract-mediated ZnO nanoparticles: microwave-assisted synthesis, characterization and antidiabetic activity evaluation.* Artificial Cells, Nanomedicine, and Biotechnology, 2018. **46**(4): p. 730-739.
101. Adhikari, S.P., et al., *One pot synthesis and characterization of Ag-ZnO/g-C3N4 photocatalyst with improved photoactivity and antibacterial properties.* Colloids and Surfaces A: Physicochemical and Engineering Aspects, 2015. **482**: p. 477-484.
102. Elumalai, K. and S. Velmurugan, *Green synthesis, characterization and antimicrobial activities of zinc oxide nanoparticles from the leaf extract of Azadirachta indica (L.).* Applied Surface Science, 2015. **345**: p. 329-336.
103. Ahamed, M., et al., *Synthesis, Characterization, and Antimicrobial Activity of Copper Oxide Nanoparticles.* Journal of Nanomaterials, 2014. **2014**: p. 1-4.
104. Abraham, N., et al., *Dye sensitized solar cells using catalytically active CuO-ZnO nanocomposite synthesized by single step method.* Spectrochimica Acta Part A: Molecular and Biomolecular Spectroscopy, 2018. **200**: p. 116-126.
105. Gawade, V., et al., *Green synthesis of ZnO nanoparticles by using Calotropis procera leaves for the photodegradation of methyl orange.* Journal of Materials Science: Materials in Electronics, 2017. **28**(18): p. 14033-14039.
106. Ruan, S., et al., *A Z-scheme mechanism of the novel ZnO/CuO n-n heterojunction for photocatalytic degradation of Acid Orange 7.* Materials Science in Semiconductor Processing, 2020. **107**: p. 104835.
107. Ramesh, M., M. Anbuvannan, and G. Viruthagiri, *Green synthesis of ZnO nanoparticles using Solanum nigrum leaf extract and their antibacterial activity.* Spectrochimica Acta Part A: Molecular and Biomolecular Spectroscopy, 2015. **136**: p. 864-870.
108. Vanathi, P., et al., *Biosynthesis and characterization of phyto mediated zinc oxide nanoparticles: a green chemistry approach.* Materials Letters, 2014. **134**: p. 13-15.
109. Bajiri, M.A., et al., *CuO/ZnO/g-C3N4 heterostructures as efficient visible light-driven photocatalysts.* Journal of Environmental Chemical Engineering, 2019. **7**(5): p. 103412.
110. Kadhem, H. and H. AL-Mathkhury, *Inhibitory effect of menthol extracted from Mentha rubra on methicillin-resistant Staphylococcus aureus.* Worl Exp Bioc, 2015. **3**(2): p. 150-54.

111. Pramila, D., et al., *Phytochemical analysis and antimicrobial potential of methanolic leaf extract of peppermint (Mentha piperita: Lamiaceae).* Journal of Medicinal Plants Research, 2012. **6**(2): p. 331-335.
112. G.K, P., et al., *In vitro antibacterial and cytotoxicity studies of ZnO nanopowders prepared by combustion assisted facile green synthesis.* Karbala International Journal of Modern Science, 2015. **1**(2): p. 67-77.
113. Fardood, S.T., et al., *Green synthesis of zinc oxide nanoparticles using arabic gum and photocatalytic degradation of direct blue 129 dye under visible light.* Journal of Materials Science: Materials in Electronics, 2017. **28**(18): p. 13596-13601.
114. Jamdagni, P., P. Khatri, and J. Rana, *Green synthesis of zinc oxide nanoparticles using flower extract of Nyctanthes arbor-tristis and their antifungal activity.* Journal of King Saud University-Science, 2018. **30**(2): p. 168-175.
115. Chitra, K. and G. Annadurai, *Antimicrobial activity of wet chemically engineered spherical shaped ZnO nanoparticles on food borne pathogen.* International food research journal, 2013. **20**(1).
116. Sherly, E.D., J.J. Vijaya, and L.J. Kennedy, *Visible-light-induced photocatalytic performances of ZnO–CuO nanocomposites for degradation of 2,4-dichlorophenol.* Chinese Journal of Catalysis, 2015. **36**(8): p. 1263-1272.
117. Manzoor, M.F., et al., *Enhanced photocatalytic activity of hydrogen evolution through Cu incorporated ZnO nano composites.* Materials Science in Semiconductor Processing, 2020. **120**: p. 105278.
118. Singh, J. and R.K. Soni, *Controlled synthesis of CuO decorated defect enriched ZnO nanoflakes for improved sunlight-induced photocatalytic degradation of organic pollutants.* Applied Surface Science, 2020. **521**: p. 146420.
119. Singh, J., et al., *The potential of green synthesized zinc oxide nanoparticles as nutrient source for plant growth.* Journal of Cleaner Production, 2019. **214**: p. 1061-1070.
120. Xu, K., et al., *Ag–CuO–ZnO metal–semiconductor multiconcentric nanotubes for achieving superior and perdurable photodegradation.* Nanoscale, 2017. **9**(32): p. 11574-11583.

121. Saravanakkumar, D., et al., *Synthesis and characterization of ZnO–CuO nanocomposites powder by modified perfume spray pyrolysis method and its antimicrobial investigation.* Journal of Semiconductors, 2018. **39**(3): p. 033001.
122. Mittal, M., M. Sharma, and O. Pandey, *UV–Visible light induced photocatalytic studies of Cu doped ZnO nanoparticles prepared by co-precipitation method.* Solar Energy, 2014. **110**: p. 386-397.
123. Wang, J., et al., *Oxygen vacancy induced band-gap narrowing and enhanced visible light photocatalytic activity of ZnO.* ACS applied materials & interfaces, 2012. **4**(8): p. 4024-4030.
124. Harish, S., et al., *Controlled structural and compositional characteristic of visible light active ZnO/CuO photocatalyst for the degradation of organic pollutant.* Applied Surface Science, 2017. **418**: p. 103-112.
125. Li, G., et al., *Role of surface/interfacial Cu2+ sites in the photocatalytic activity of coupled CuO− TiO2 nanocomposites.* The Journal of Physical Chemistry C, 2008. **112**(48): p. 19040-19044.
126. Taufik, A., A. Albert, and R. Saleh, *Sol-gel synthesis of ternary CuO/TiO 2 /ZnO nanocomposites for enhanced photocatalytic performance under UV and visible light irradiation.* Journal of Photochemistry and Photobiology A: Chemistry, 2017. **344**: p. 149-162.
127. Xu, L., et al., *Improved photocatalytic activity of nanocrystalline ZnO by coupling with CuO.* Journal of Physics and Chemistry of Solids, 2017. **106**: p. 29-36.
128. Khang, N.C., *Further Investigation and Analysis on the Origin of the Optical Properties of Visible Hetero-photocatalyst TiO 2/CuO.* Journal of Electronic Materials, 2017. **46**(10): p. 5497-5502.
129. Sherly, E., J.J. Vijaya, and L.J. Kennedy, *Visible-light-induced photocatalytic performances of ZnO–CuO nanocomposites for degradation of 2, 4-dichlorophenol.* Chinese Journal of Catalysis, 2015. **36**(8): p. 1263-1272.
130. Xiao, Q., et al., *Photocatalytic decolorization of methylene blue over monoclinic pyrochlore-type Pb2Nb2O7 under visible light irradiation.* Journal of Alloys and Compounds, 2009. **468**(1-2): p. L9-L12.

131. Saleh, R. and N.F. Djaja, *Transition-metal-doped ZnO nanoparticles: synthesis, characterization and photocatalytic activity under UV light.* Spectrochimica Acta Part A: Molecular and Biomolecular Spectroscopy, 2014. **130**: p. 581-590.
132. Saleh, R. and N.F. Djaja, *UV light photocatalytic degradation of organic dyes with Fe-doped ZnO nanoparticles.* Superlattices and Microstructures, 2014. **74**: p. 217-233.
133. Chai, B., et al., *In-situ synthesis of WO3 nanoplates anchored on g-C3N4 Z-scheme photocatalysts for significantly enhanced photocatalytic activity.* Applied Surface Science, 2018. **448**: p. 1-8.
134. Renuka, L., et al., *Synthesis of Sunlight Driven ZnO/CuO Nanocomposite: Characterization, Optical, Electrochemical and Photocatalytic Studies.* Materials Today: Proceedings, 2017. **4**(11): p. 11782-11790.
135. Harish, S., et al., *Controlled structural and compositional characteristic of visible light active ZnO/CuO photocatalyst for the degradation of organic pollutant.* Applied Surface Science, 2017. **418**: p. 103-112.
136. Koffyberg, F. and F. Benko, *A photoelectrochemical determination of the position of the conduction and valence band edges of p-type CuO.* Journal of Applied Physics, 1982. **53**(2): p. 1173-1177.
137. Nair, M., et al., *Chemically deposited copper oxide thin films: structural, optical and electrical characteristics.* Applied Surface Science, 1999. **150**(1-4): p. 143-151.